Bulgarian Academy of Sciences ISSN 1311-753X

Bulgarian Geophysical Journal

2004, Vol. 30, 1-4.

Special issue:

Papers presented at European Geosciences Union (EGU) 1st General Assembly, Nice, 26-30 April 2004
Guest Editors: Dr. Bruno Zolesi and Dr. Ljiliana Cander

The issue was supported by Ministry of Education and Science of Bulgaria - National Science Fund

CONTENTS

INCLUDING THE GALLAGHER PLASMASPHERIC MODEL IN THE NEQUICK IONOSPHERIC MODEL

M. Cueto[1], P. Coisson[2], S. M. Radicella[2], L. Ciraolo[3], M. Herraiz[1]

[1]Department of Physic of the Earth, Astronomy and Astrophysic I, Universidad Complutense de Madrid, Avenida Complutense s/n 28040, Madrid, Spain,
e-mail: mcs@fis.ucm.es, mherraiz@fis.ucm.es
[2]Aeronomy and Radiopropagation Laboratory, Abdus Salam ICTP, 34100 Trieste, Italy,
e-mail: rsandro@ictp.it, coissonp@ictp.it
[3]Istituto di Fisica Applicata Carrara, CNR, Via Panciatichi 64, Firenze, Italy,
e-mail: l.ciraolo@ifac.cnr.it

Abstract. The NeQuick ionospheric electron density model has a very simple topside formulation which allows to take into account the electron content up to 20000 km. In the present work Gallagher model has been used in connection with NeQuick to provide a more realistic representation of the electron concentration distribution in the plasmasphere. Electron density profiles and TEC values obtained by NeQuick alone and by NeQuick+Gallagher have been compared. ISIS-2 topside sounder profiles have been used for comparison of electron density at 1300 km. In addition, GPS vertical TEC values obtained from data of the San Fernando IGS station (36.46 N, 353.79 E) have been compared with the NeQuick and NeQuick+Gallagher vertical TEC values.

Keywords: ionosphere, plasmasphere, electron density, total electron content

1. Introduction

The NeQuick model is one of the three electron density models developed at the Abdus Salam ICTP in Trieste and the Institute for Meteorology and Geophysics in Graz (Hoccheger et al., 2000; Radicella and Leitinger, 2001). All three are based on the DGR "profiler" concept (Di Giovanni and Radicella, 1990) further developed by Radicella and Zhang (1995) and calculate electron density values as a function of solar activity, month, UT, height and geographic coordinates. The "quick calculation" model NeQuick uses a simple formulation for the topside F layer, which is essentially a semi-Epstein layer with a thickness parameter which increases linearly with height. A NeQuick model demo version is available online on the website http://arpl.ictp.trieste.it/.

The Gallagher model (Gallagher et al., 1988) has been used in connection with NeQuick to search a more realistic representation of the electron concentration distribution in the plasmasphere.

The Gallagher model is an empirical model of plasmaspheric low energy plasma consisting of H+. It was developed from a data base derived from measurements taken by the Retarding Ion Mass Spectrometer, RIMS (Chappell et al., 1981), on the Dynamics Explorer 1 satellite and represents the plasmasphere from 0 to 12 hours magnetic local time. The Gallagher plasmaspheric model calculates electron density values as a function of the day of the year, UT, height and geographic coordinates.

2. Comparison with ISIS2 electron densities

In order to study the behavior of NeQuick and Gallagher models at pla-

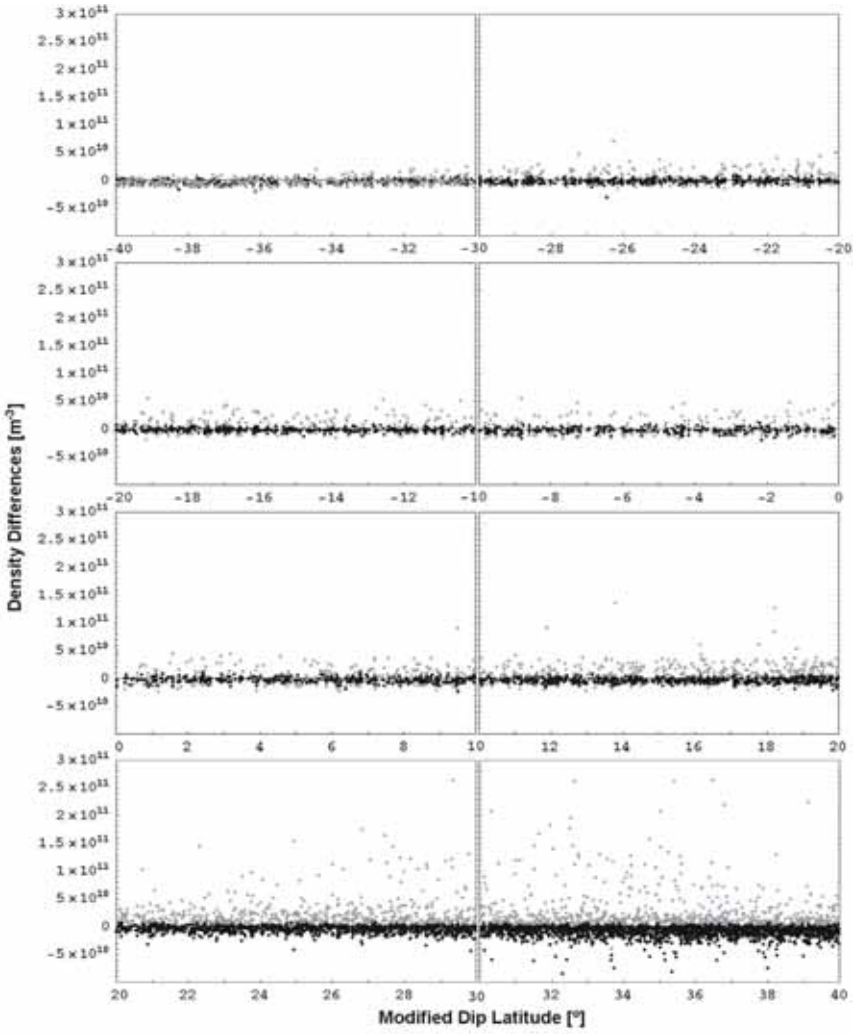

Fig. 1. Differences between NeQuick and ISIS2 (grey points) and between Gallagher and ISIS2 electron density values (black points) as a function of modified dip latitude at 1300 km.

smaspheric heights, NeQuick and Gallagher electron density values have been compared with those derived from measurements taken by the ISIS2 satellite at 1300 km. The ISIS 2 satellite was designed and operated jointly by USA and Canada to investigate the topside ionosphere using remote sensing and in-situ instruments (Bilitza, 2003). All ISIS2 data are archived at the National Space Science Data Centre and are available online on NSSDC's anonymous ftp site (ftp://nssdcftp.gsfc.nasa.gov/spacecraft_data).

The selected electron density values correspond to 1972-1983. All data are day-time ones (between 6:00 and 20:00 LT) and between ±40º modified dip latitude. The modified dip latitude μ , introduced by Rawer (1963), is defined as:

$$\tan \mu = I/\sqrt{\cos \varphi} \qquad (1)$$

I being the true magnetic dip in the ionosphere (usually at 300 km). In the equatorial zone the lines of constant μ are practically identical to those of magnetic inclination I, but with increasing latitude they deviate and come nearer to those of constant geographic latitude φ, and the poles are identical to the geographical ones.

In this comparison the NeQuick model is driven by the daily 10.7 cm solar radio flux values to obtain from ITU-R (former CCIR, Bilitza et al., 1993) global coefficients the foF2 and M3000 ionospheric characteristics. Differences between modelled and experimental values have been calculated after subdividing data according to their modified dip latitude.

Results for the modified dip latitude range ±40º at intervals of 10 degrees are shown in Figure 1.

The spread of the electron density differences at 1300 km between Gallagher and ISIS2 are smaller than those obtained with the NeQuick model for all intervals. This result confirms the importance of including a more realistic representation of the electron concentration distribution of the plasmasphere in the NeQuick model.

3. Transition region used

In order to connect the NeQuick vertical profile to the Gallagher model, a transition region has been used. The transition region between the NeQuick based region (from the earth surface to a height hi above the F2 electron density peak height) and the Gallagher region (from 1300 km up) should verify that the profile shape is well reproduced, without gradient discontinuities in the function and in its first derivative. Consequently it is necessary to choose a transition function, $f_3\,(h)$, which verifies

$$\begin{aligned} f_3\,(hi) &= NeQ(hi) \\ f_3\,(1300) &= Gal(1300) \\ f_3'\,(hi) &= NeQ'(hi) \\ f_3'\,(1300) &= Gal'(1300) \end{aligned} \qquad (2)$$

where *hi* is the lower height of the transition region, *NeQ(hi)* is the NeQuick density at *hi*, *Gal*(1300) is the Gallagher density at 1300 km height,

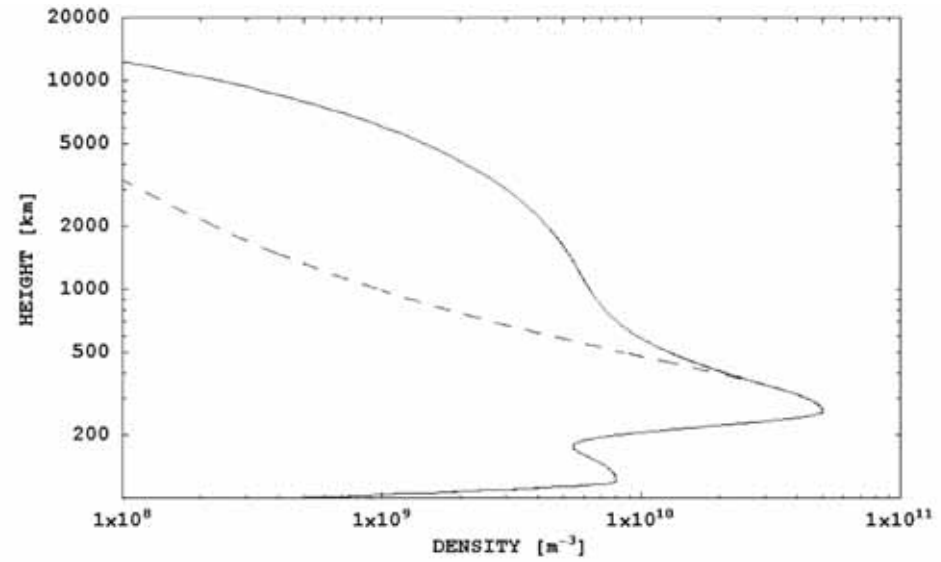

Fig. 2. Example of NeQuick and NeQuick+Gallagher electron density profile using a bilogarithmic scale for July 1996 at 6:00 UT and geographic coordinates (40.0ºS,354ºE). Solid line: NeQuick+Gallagher electron density profile; Dashed line: NeQuick electron density profile. hi is the altitude where the two curves depart from each other (350 km in this case).

NeQ'(hi) is the NeQuick model slope at hi and *Gal'*(1300) is the Gallagher slope at 1300 km height. The value of *hi* is not the same for all case: it should verify that *NeQ(hi)* is higher than *Gal*(1300) to provide a well reproduced transition region shape. Consequently, hi has been selected as the height (above the F2 electron density peak height) where the electron density is equal to 0.75Nmax, with Nmax the F2 peak electron density. Another essential condition that the selected function should fulfil is that the transition region does not show any density increase with height, which would have no physical meaning.

From all the candidates considered, the function that fits what we need is a function of the type:

$$f_3(h) = a + \frac{b}{h} + \frac{c}{h^2} + \frac{d}{h^3} \qquad (3)$$

where *h* is height and a, b, c and d are four coefficients which will be fixed solving the equation system given by (2).

An example of NeQuick and NeQuick+Gallagher electron density profiles is given in Figure 2 (a bilogarithmic scale is used to show clearly the differences between both profiles).

4. Vertical TEC comparison

NeQuick and NeQuick+Gallagher vertical total electron content (vTEC)

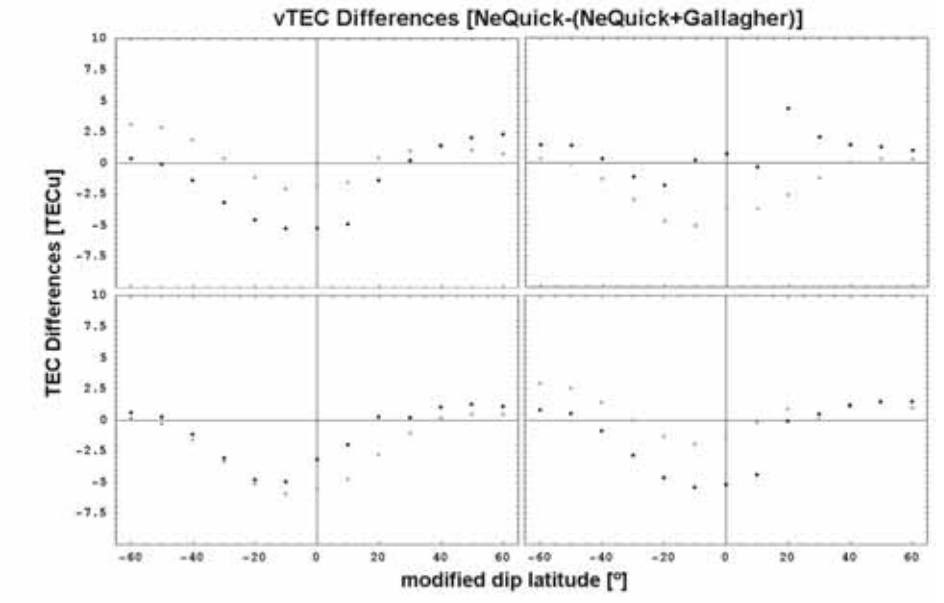

Fig. 3. vTEC differences between NeQuick and NeQuick+Gallagher between 0-20000 km for a geographic longitude of 354º as a function of geographic latitude. Black points: results at 12:00 UT; Grey points: results at 00:00 UT. Upper row: January 1996 (left) and July 1996 (right); Lower row: April 1996 (left) and October 1996 (right).

values between 0-20000 km height for a geographic longitude of 354º (which approximately corresponds to that of the San Fernando IGS station, Spain) at geographic latitude intervals of 10º have been calculated. Four months (January, April, July and October, which represent the four seasons) and two hours (0:00 and 12:00 UT) of 1996 (a year of low solar activity) have been considered. Results for the geographic range ±60º are shown in Figure 3. The latitude of the magnetic equator for a geographic longitude of 354º is 10.79º S.

The behavior in January, July and October is similar at 12:00 UT, with the NeQuick model alone providing lower values than the NeQuick + Gallagher at low latitudes but very close values at middle latitudes. There are little differences in April and only in the Northern equatorial anomaly region is shown a value of NeQuick + Gallagher 5 TEC units below the NeQuick alone.

Differences between both models in April and July are similar at 0:00 UT: again the NeQuick model alone provides lower values than the NeQuick + Gallagher at low latitudes. Values of vTEC at middle latitudes are very close. The behavior of NeQuick and NeQuick+Gallagher models is similar in January and October, showing smaller vTEC differences between both models than those obtained at 12:00.

5. Comparison with GPS vertical values from San Fernando IGS station

GPS vTEC values from San Fernando IGS (International GPS Service)

station (36.46 N, 353.79 E) between 0-20000 km height have been compared with those obtained with NeQuick and NeQuick+Gallagher.

In order to calculate GPS vTEC of San Fernando IGS station, the following procedure has been carried out:

- GPS data for the requested period were downloaded from the IGS archive.
- Differential phase delays (DPDs) and differential group delays (DGDs) were computed.
- DPDs were leveled to DGDs in order to consider one constant bias for each station and satellite.
- A single-day, single-station solution was calculated based on the following assumptions: a) Ionosphere was assumed to be a thin shell at a height of 400 km; b) Slant TECs were mapped to vTECs by sec(χ) (χ being the angle between the ray GPS satellite-IGS station and the local vertical in the piercing point between the ray itself and the shell); and c) vTEC on the shell was assumed to be described by a polynomial in local time and Rawer's modified dip latitude at the piercing point.

Eight quiet days of 1996 (11 and 21 of April, 1, 11 and 21 of July, 1, 11 and 21 of October) have been selected, and vTEC every 10 minutes for each day has been calculated. Results for 11 of July and 21 of October are shown in Figure 4.

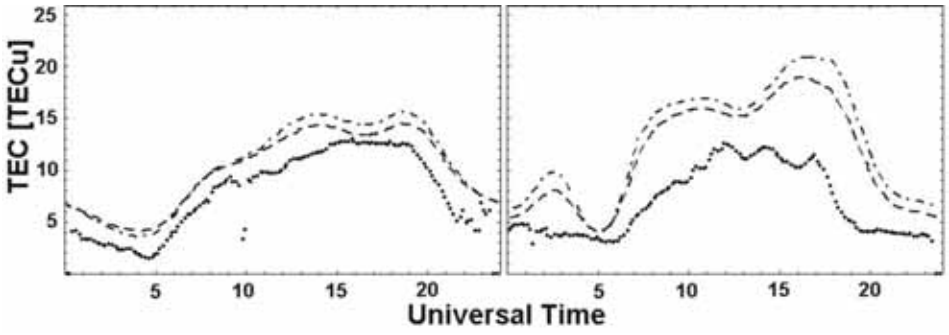

Fig. 4. NeQuick (dotted-dashed line), NeQuick+Gallagher (dashed line) and GPS (dotted line) vTEC values as a function of Universal Time for San Fernando IGS station, July 11th 1996 (left panel) and October 21st 1996 (right panel).

NeQuick+Gallagher vTEC values tend to be slightly closer to the experimental ones than the NeQuick model in all cases. Differences between both models are very small (no higher than 2 TECu). This is consistent with the fact that San Fernando IGS station is located at mid-latitude: differences between vTEC values for those latitudes are not expected to be higher than 2.5 TECu (see the previous section).

In this comparison the NeQuick and NeQuick+Gallagher models are driven by the daily 10.7 cm solar radio flux values to obtain from ITU-R global coefficients the foF2 and M3000 ionospheric characteristics. Differences between modelled and GPS vTEC values are supposed to decrease if experimental f0F2 and M3000 values are used as input in both models. A further comparison between theoretical and GPS vertical TEC values using foF2 and

M3000 peak values obtained from experimental ionograms will be done to clarify the point.

6. Conclusions

The comparison between NeQuick and NeQuick+ Gallagher density and vertical TEC values has shown that:

1. The spread of the electron density differences at 1300 km between Gallagher and ISIS2 are smaller than those obtained with the NeQuick model. It is important to point out that in this comparison the NeQuick model is driven by the daily 10.7 cm solar radio flux values to obtain from ITU-R global coefficients the foF2 and M3000 ionospheric characteristics. A further analysis using ISIS2 NmF2 and hmF2 values will be done to verify the results shown in this work.

2. The latitudinal variation of the vTEC differences (NeQuick+Gallagher)-NeQuick depends on the selected month and UT. It is worth noticing that 1996 is a year of low solar activity. Differences for high solar activity are expected to be higher than those shown here.

3. NeQuick+Gallagher vTEC values are higher than NeQuick vTEC values for low latitudes, indicating a plasmaspheric contribution at those latitudes not properly shown by NeQuick.

5. Comparisons of NeQuick and NeQuick+Gallagher with experimental vTEC in San Fernando, a mid-latitude station, show that NeQuick+Gallagher vTEC tends to be slightly closer to the experimental values than the NeQuick model. A further comparison between theoretical and GPS vertical TEC values using foF2 and M3000 peak values from ionosondes will be done to verify these results.

7. References

Bilitza D., K. Rawer, L. Bossy, T. Gulyaeva, 1993. International Reference Ionosphere - past, present and future: I. electron density. Adv. Space Res., 13, No 3, 3-13.

Bilitza D., B. Reinisch, R. Benson, J. Grebowsky, N. Papitashvili, X. Huang, W. Schar and K. Hills, 2003. Online database of satellite sounder and insitu measurements covering two solar cycles. Adv. Space Res., 31 (3), 769-774.

Chappell, C. R., S. A. Fields, C. R. Bauher, J. H. Hoffmann, W. B. Hanson, W. W. Wright, H. D. Hammack, G. R. Carignan and A. F. Nagy, 1981. The retarding ion mass spectrometer on Dynamics Explorer-A. Space Csi. Instrum., 5, 477-491.

Di Giovanni, G. and S. M. Radicella, 1990. An analytical model of the electron density profile in the ionosphere. Adv. Space Res., 10, No 11, 27-30.

Gallagher, D. L., P. D. Craven and R. H. Comfort, 1988. An empirical model of the Earth?s plasmasphere, Adv. Space Res., 8, No 8, 15-24.

Hochegger, G., B. Nava, S. Radicella and R. Leitinger, 2000. A family of ionospheric models for different uses. Phys. Chem. Earth (C), 25, No 4, 307-310.

Radicella, S. M. and Man-Lian Zhang, 1995. The improved DGR analytical model of electron density height profile and total electron content in the ionosphere. Annali di Geofisica, 38, No 1, 35-41.

Radicella, S. M. and R. Leitinger, 2001. The evolution of the DGR approach to model electron density profiles. Adv. Space Res., 27, No 1, 35-40.

Rawer, K., 1963. Meteorological and astronomical influences on radio wave propagation. Ed. B. Landmark, Academy Press, New York.

STORM-TIME CHANGES IN IONOSPHERIC TEC DURING THE DISTURBANCES ON THE NOVEMBER 5-7, 2001 STORM

A. Krankowski[1], I.I. Shagimuratov[2], L.W. Baran[1], G.A. Yakimova[2], A.V. Radievsky[2]

[1]Institute of Geodesy, University of Warmia and Mazury in Olsztyn, Oczapowski St. 1, 10-957 Olsztyn, Poland, e-mail: kand@uwm.edu.pl
[2]WD IZMIRAN, Kaliningrad, Russia

Abstract. This paper presents the response of the ionospheric total electron content over Europe to the severe storm on November 5-7, 2001 (Σ Kp = 54). Spatial and temporal changes in TEC we analyzed on the basis of TEC maps. The maps were compiled using GPS measurements from 70 - 90 stations of the International GPS Service (IGS) / EUREF Permanent Network (EPN). Our estimation technique provided TEC maps with 15 min intervals and spatial resolution of 150 - 300 km.
One of the features of the developing winter storm over Europe was a positive effect observed at night, at its early stage. This positive effect was recorded only at latitudes higher than 50N. TEC enhancements exceeded 150% relative to a quiet day. The strong enhancement of TEC was probably connected with particle precipitation.
A long-lasting negative perturbation was registered in the daytime on November 6 and 7, 2001. The depression of TEC reached 70 - 100%. TEC maps showed that the spatial distribution of TEC underwent dramatic variations. In the ionosphere large- and medium-scale structures, including both increases and decreases in TEC, develop during the storm. TEC maps were used for an analysis of the dynamics of latitude profiles. The latitude dependence of TEC is significantly modified during a storm. The latitudinal profiles very well represent the dynamics of a mean ionospheric trough (MIT). During the storm the trough was displayed at a latitude of about 48N.

Key words: ionosphere, TEC, geomagnetic storms, GPS.

1. Introduction

Geomagnetic storms include a competition of many different and interacting processes in the magnetosphere-ionosphere-thermosphere system. These complex phenomena need comprehensive measurements of ionospheric parameters on a global scale. Until now, the analysis of ionospheric storms was mainly based on ionosonde data and TEC measurements, using the

Faraday effect on the signals of geostationary satellites. During the storm ionosonde measurements at high latitudes often cannot provide complete information about the state of the ionosphere. In contrast to them, Global Positioning System (GPS) observations enable TEC measurements in most conditions. Today the International GPS Service (IGS) / EUREF Permanent Network (EPN) is broader and denser than the ionosonde one. Recently GPS measurements were used to study the storms in November 1994 (Ho et al., 1996), on 18-19 October 1995 (Lu et al., 1998), in January 1997 (Ho et al., 1998; Jakowski et al., 1999; Lu et al., 2001), in November 1997 (Baran et al., 2001) in September 1999 (Shagimuratov et al., 2002) and in March-April 2001 (Krankowski et. al., 2005).

This paper presents an analysis of the TEC behavior over the European sector during the severe storm on November 5-7, 2001.

2. Data and method of TEC estimation

GPS observations collected at IGS/EPN were used to create TEC maps. More than 80 stations were included in the analysis of the response of TEC to a geomagnetic storm.

While estimating TEC from GPS observations, the ionosphere was approximated by a spherical shell at a fixed height of 400 km above the Earth's surface. The simple geometric factor was used to convert the slant TEC into a vertical one (Mannucci et al., 1998; Wanninger et al., 1994; Wilson et al, 1995). High-precision phase measurements were used while processing. The phase ambiguities were removed by fitting phase measurements to the code data collected along an individual satellite pass. After pre-processing the phase measurements contained an instrumental bias only (Baran et al, 1997; Coco et al, 1991; Wilson and Mannucci, 1993). The biases were determined for each station using GPS measurements of all satellite passes over a given site in a 24-hour period. The diurnal variations of TEC over a site and the biases for all satellites were estimated simultaneously. At all stations, before the technique had been run, the instrumental biases were removed in all satellite passes. Using this procedure an absolute line of sight TEC for all satellite-receiver paths was calculated.

In order to obtain the spatial and temporal variation of TEC and to create TEC maps the measurements were fitted to a spherical harmonic expansion in a geographic latitude (Φ) and longitude (Θ). The spherical harmonic expansion was truncated to the order and degree of 16. The accuracy of TEC maps depends on spatial gaps in TEC data (Mannucci et al., 1998). The large number of GPS stations in Europe provides a good coverage for GPS data and enable to get high-accuracy TEC maps with an error at a level of 1 - 3 TECU (Baran and Shagimuratov, 1998; Wanninger et al., 1994; Wilson et al, 1995; Zarroa and Sardon, 1996). The coverage is a very adequate shell and yields a reasonable surface harmonic fit, providing TEC maps with a spatial resolution of 100-300 km and a time resolution of 15 min.

In order to determine the ionospheric deviations during the storm the percentage change of storm-time TEC relative to TEC maps for quiet conditions was computed. To obtain the quiet time conditions (quiet day) we averaged 5 previously magnetically quiet days of TEC measurements. The maps over Europe in this case were produced every 15 minutes. To discuss the storm

behavior in detail, various temporal and TEC latitudinal profiles were obtained from GPS maps.

3. Geomagnetic conditions

An intensive geomagnetic storm took place on November 5 - 7, 2001. The main phase of the storm started about 00 UT on November 6. The Dst index reached its minimum value - 270 nT at 03 UT on November 6 (Figure 1.) Simultaneously the Kp index amounted to 9 and ΣKp∼54. The recovery phase took place after 15:00 UT on November 8, when Dst slowly returned to its regular level.

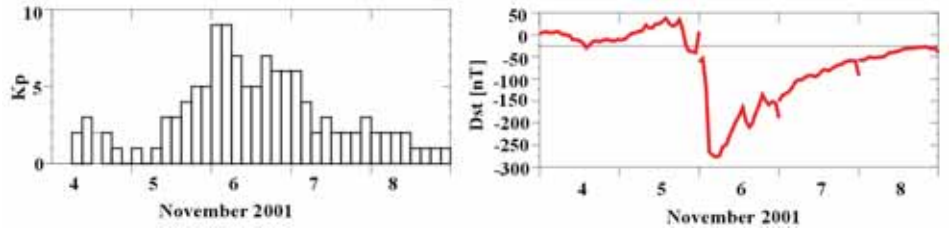

Fig.1. Variations of Kp and Dst index during 4 - 8 November 2001.

4. Results of observations and discussion

4.1. Storm-time dynamics of diurnal variations of TEC

A general idea of storm development can be got from day-by-day diurnal variations of TEC. The evaluation of diurnal variations of TEC at different latitudes during the storm of November 5 - 8 2001 is presented in Figure 2. It shows the variations of TEC over individual European stations at a latitude range from 40º N (down) to 70º N (top) around a longitude of 20º E.

At auroral and subauroral stations (Tromsoe - TROM, Kiruna - KIRU, Vilhelmina - VIL0, Vaasa - VAAS), as well as at the mid-latitude station of Onsala (ONSA), a surge of TEC enhancement were detected in diurnal variations before the main phase of the storm (Figure 2). In the auroral region the night enhancement of TEC was more pronounced. The amplitude of the surge decreased towards lower latitudes. Time delays of the surge of lower latitude stations relative to high latitude ones can be easily recognized in Figure 2.

It is a well-known fact that the occurrence of geomagnetic storms in the ionosphere depends on the season (Fuller-Rowell et al., 1996). An ionospheric storm usually consists of a positive phase (enhancement of electron density relative to quiet conditions) and a negative phase (depression of electron density) (Lastovicka, 2002; Lu et al., 2001 and Tsagouri et al., 2000). At middle latitudes the negative phase is more pronounced in summer in opposition to the winter positive phase. The storm-time auroral energy input results in traveling ionospheric disturbances (TIDs) during the storm onset, and disturbed global wind circulation (Forster et al., 1999). At mid-latitudes the positive effect can be attributed to TID (Prolss, 1993). The velocity of large-scale

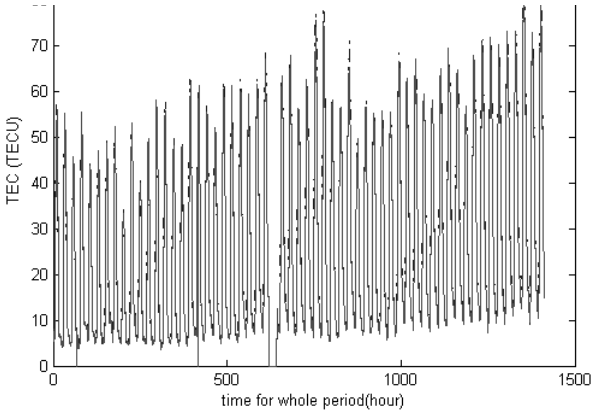

Fig.2. Diurnal variations of TEC at different latitudes during storm of 5 - 8 November 2001

traveling disturbances can reach 400-700 m/s (Jakowski et al., 1999; Baran et al., 2001). The speed of the discussed surge of TEC enhancement was less than 100 m/s. The observed TEC enhancement and displacement of the surge can be probably attributed to auroral particle precipitations and expansion of the auroral oval to lower latitudes in the driven phase of the geomagnetic storm.

Considerable changes in the diurnal variations of TEC were observed on November 6. A significant depression of the daytime TEC (a strong negative effect) took place during the storm. The effect was observed at all latitudes discussed, reaching the maximum value at high latitudes. During the storm the daytime level of TEC was comparable with the night TEC. TEC depression was also recorded on the second day of the storm.

Under quiet day conditions, at auroral and subauroral stations, the diurnal variations of TEC were very similarly to variations at mid-latitude stations. It is evident that the main role in producing ionization at auroral and subauroral region during quiet conditions was played by solar radiation. During the storm, dynamic processes dominated in generating diurnal varia-

tions.

It is interesting that during the storm, at high-latitude stations, the change from the daytime to night TEC started earlier than on the previous day. The reasons for the above effect are probably perturbations in Dst variations around the noon on November 6, during the recovery stage of the storm (Figure 1).

After midnight and in the morning hours on November 6/7 short-time perturbations describing the surge of TEC enhancement could be seen (Figure 2). The perturbations were observed at all latitudes (down to 36N). The maximum of TEC enhancement was simultaneously detected at all latitudes (without a time delay). On the previous and following quiet days this effect was not observed. Such an effect can be caused by the penetration of an electric field associated with substorms to middle and low latitudes (Shiokawa et al., 2000; Pi et al., 2000).

4.2. Spatial and temporal changes of TEC during a storm over Europe.

The dynamics of the spatial distribution of TEC over Europe was analyzed on the basis of TEC maps. We used differential TEC maps to study the storm-time changes of ionospheric TEC. These maps present the percentage deviation of TEC relative to quiet day - TEC*:

$$\Delta TEC = (TEC - TEC^*)/ TEC^* \ \% \qquad (1)$$

To obtain TEC of quiet day we used mean values from previous magnetically quiet days. Figures 3 present TEC maps for Europe, for November 5,

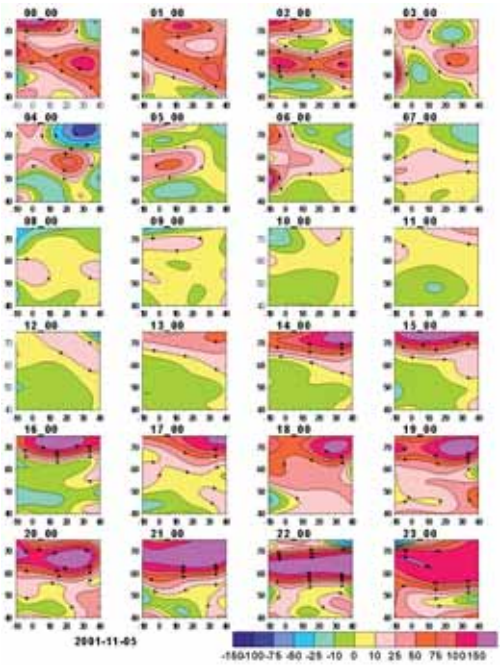

Fig.3a. The differential TEC maps over Europe for 5 November 2001

6 and 7, 2001.

Night TEC enhancement appeared after 19 UT on November 5, over all Europe. The enhancement was observed as a narrow band located at a latitude of about 68N, indicating an auroral oval of particle precipitations. In the following hours the enhancement of TEC expanded and moved down towards lower latitudes. The relative enhancement of TEC reached 100-150% with respect to the quiet days. The positive effect took place until 48ºN, but only in the western part of Europe. Thus, the response of TEC to the geomagnetic storm showed a local time dependence.

The strong relative enhancement of TEC caused both the precipitation and spatial migration of the main ionospheric trough during the disturbances. Over the storm the trough minimum shifted to the equator. At the same time the auroral oval expanded to lower latitudes.

The negative effect with a depression of TEC began in the eastern part of Europe after 05UT on November 6, to cover all Europe. The TEC depression was observed at all latitudes. The maximal effect took place in the auroral and subauroral ionosphere during the daytime on November 6 and 7. The

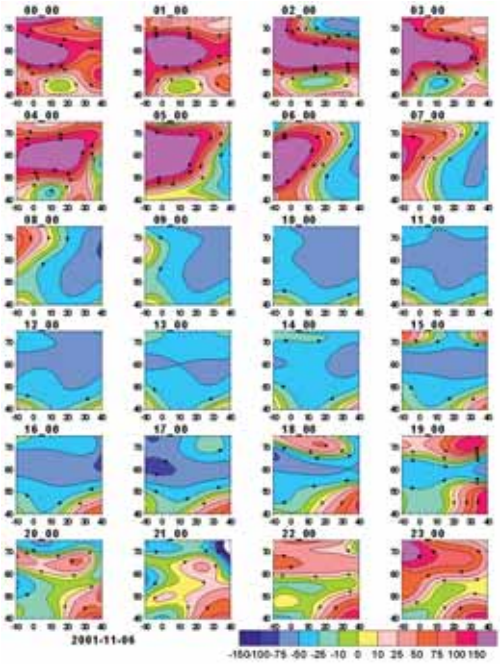

Fig.3b. The differential TEC maps over Europe for 6 November 2001.

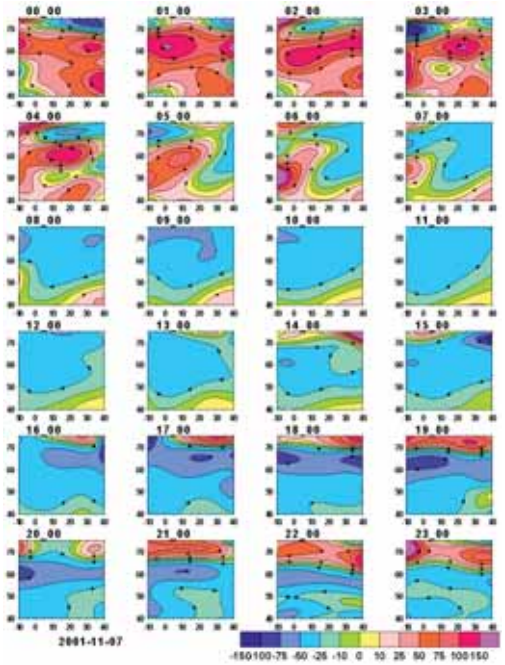

Fig.3c. The differential TEC maps over Europe for 7 November 2001.

depression of TEC makes up 50-70% at mid-latitudes and more than 100% in subauroral regions.

TEC maps show regional features of storm development. The unusual large-scale structures (wave-like depletion and increase in TEC) can be seen at 04-07 UT over Europe on November 7. The effect may be attributed to the storm-disturbed thermospheric winds. The occurrence of the mid-latitude ionospheric trough is presented on TEC maps in the afternoon.

During the storm the intensive TEC fluctuations developed in the ionosphere. Inhomogeneous structures were more pronounced in the auroral/subauroral ionosphere. The intensive irregularities were found even at middle latitudes.

Figure 4 presents TEC variations along the traces of a single satellite (PRN 14) on a quiet and disturbed day - November 5 and 6 ($\Sigma Kp \sim 54$), observed at different European stations. Since GPS satellites are in 12-side-real-hour orbits, the constellation repeats for consecutive days, except for the fact that the satellite arrived 4 min earlier each day.

The analyses of TEC variations for individual satellite passes show that during the driven phase of the storm, different scale irregularities developed in the ionosphere. Figure 4 shows that during the storm large- and medium-scale irregularities caused deep fluctuations of TEC at mid-latitude stations: Lamkowko - LAMA (53N) and Wroclaw - WROC (51N). The behavior of TEC at stations spaced out at 300-500 km was also different. It is evident that the spatial correlation of TEC deteriorated during the storm. As shown in the next section, during the November storm the ionospheric trough was

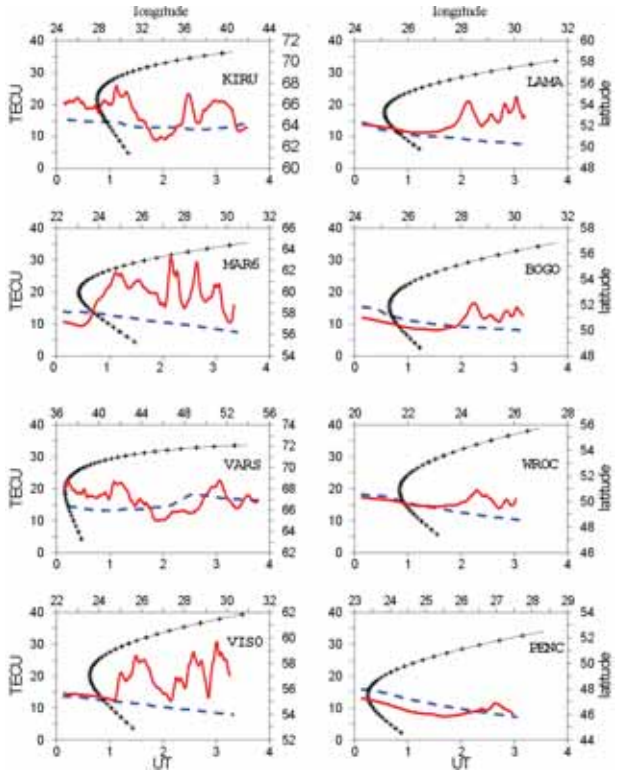

Fig 4. Temporal TEC variations along individual satellite passes for PRN 14 observed at different stations on quiet (blue) and disturbed (red) day.

observed below a latitude of about 48ºN. Ionospheric irregularities can be often observed around the trough where electron density gradients are significantly increased. This information is useful for GPS users because the horizontal ionospheric gradients can lower ambiguity resolution and affect the accuracy of GPS positioning (Wanninger, 1993; Krankowski et al., 2002).

4.3. Latitudinal variations of TEC

We used the latitude profiles obtained from TEC maps at a fixed longitude for an analysis of latitudinal TEC variations. Figure 5a presents the variations of the latitudinal profiles over Europe at the 20 ºE longitude for geographic latitudes from 40 ºN to 75 ºN on a quiet day of November 5, 2001. During a quiet day the profiles show a steady slope. TEC was virtually not varied in the daytime in the latitude range examined. During the storm the latitudinal profiles were highly modified. The latitudinal gradients were different when compared with quiet conditions (Figures 5a and 5b).

The strong TEC enhancement at high latitudes was clearly recognized in the evening of November 5. The enhancement reached the factor 3-4 relative to mid-latitudes. Night enhancements of TEC are often observed in

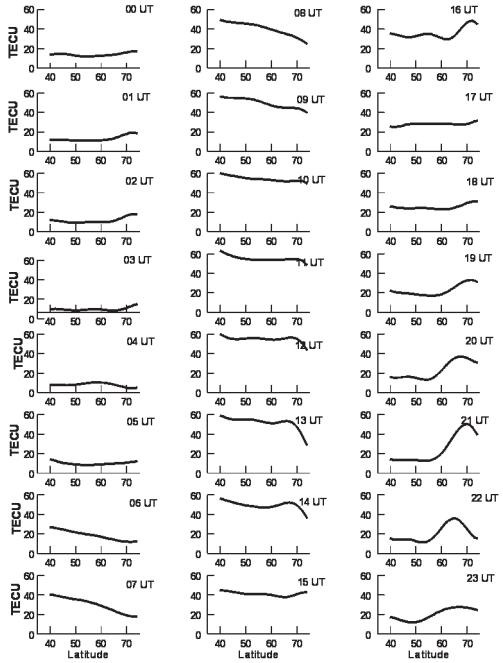

Fig 5a. Latitudinal TEC profiles for 5 November 2001 over Europe at longitude 20 E

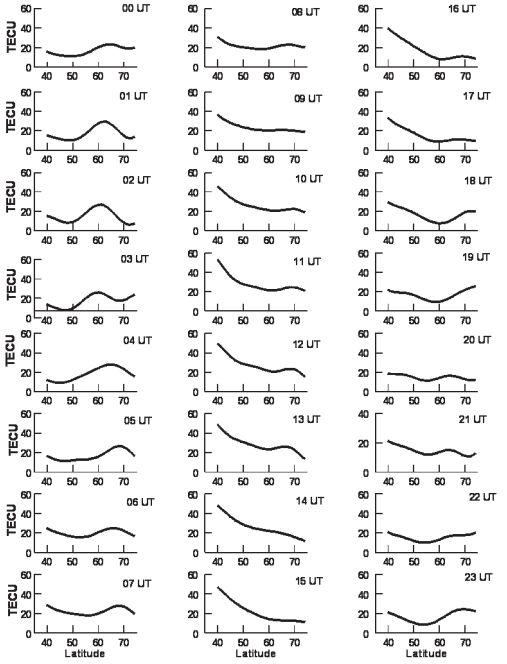

Fig 5b. Latitudinal TEC profiles for 6 November 2001 over Europe at longitude 20 E.

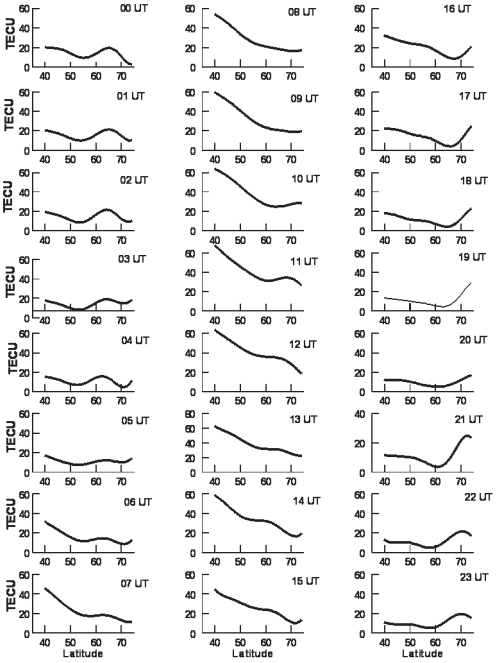

Fig 5c. Latitudinal TEC profiles for 7 November 2001 over Europe at longitude 20 E.

November GPS data, but the maximum of TEC enhancement occurred at latitudes higher than 70N. Usually it does not exceed the factor 1.5-2.0. The maximum of TEC enhancement occurred at lower latitudes and displaced in time to the equator (Figure 5a). As already mentioned, this effect can be attributed to particle precipitation and the expansion of the auroral oval to lower latitudes.

After midnight on November 6/7, the latitudinal TEC profiles showed a striking structure recognized as the mid-latitude ionospheric trough (Wielgosz at al., 2004). The trough was shifted in time and in the morning reached a latitude of 48N. The polar wall of the trough became more pronounced. The ratio of the minimum TEC level to the polar wall value was 2-3. At 01-04UT on November 6, a trough-like structure was also seen at higher latitudes (near 70N). This structure was probably a high-latitude trough. (Werner and Prolss, 1997).

In the day-time, during the negative phase of the storm, latitudinal gradients increased. The TEC decreased towards higher latitudes. It shows that the depression of ionization during the storm was more significant at higher latitudes. After 15UT the latitudinal profiles again represented a trough-like structure.

On the second day of the storm the latitudinal TEC variations were similar to the previous day, i.e. November 6. We discussed the day-time TEC increase in relation to the previous day at lower latitudes, but at higher latitudes the low level of TEC was maintained. After the noon the profiles represented a mid-latitude trough with a sharp polar wall. The dynamics of the

trough at 14-23 UT is well described by these profiles. During this period, the trough was detected from 70N to 58N.

5. Conclusion

Using observations based on the worldwide GPS network, we found the following morphological features of the TEC behavior on a global scale (European sector) during the storm of November 5, 6, 7, 2001:

1) The storm began with a short-time positive phase. The maximum of the positive effect took place in the auroral and subauroral ionosphere. The strong - relative to quiet conditions - enhancement of TEC (~150%) at high latitudes can be attributed to such processes as: particle precipitations, auroral oval expansion, as well as storm-time migration of the ionospheric trough.

2) A long-lasting negative effect took place during the daytime on November 6 and 7, 2001. The TEC depression reached 60-70%.

3) The high deviation of TEC relative to quiet conditions gave rise to the displacement of the main ionospheric through, which was recognized after midnight on November 6 around a latitude of 50N.

4) During the storm intensive large-scale irregularities were observed even at mid-latitudes in the ionosphere.

5) The regional features of the response of the ionosphere to geomagnetic storms are clearly visible.

We previously analyzed a storm of November 22, 1997 (Baran et al., 2001). This storm was less intensive (Dst ~130nT) and took place near solar minimum in contrast to the storm discussed in this paper (Dst~270nT), which occurred at solar maximum. Both storms started about at the some time. It is quite interesting that the response of the ionosphere to storms was completely different. In contrast to the above-described storm, the previous one was characterized by a strong long-lasting positive effect at middle/low latitudes. Further, detailed investigations of the response of the ionosphere to similar geomagnetic storms are needed and will be carried out in the future.

The behaviors described here are definitely not new in the literature, and should have been expected. Nevertheless, we stress here that they have been found by using GPS-TEC data downloadable as Rinex files. In principle, one should be quite aware of how far the Rinex file data are from being a physical measure of the "real" total electron contents (Mannucci et al., 1998: Wilson and Mannucci, 1993; Coco et al, 1991). Despite this problems related in principle to the use of GPS TEC data, the results found here are very sensible.

This is a strong and encouraging indication: indeed, our findings seem to indicate that physically sensible observations on the ionospheric response to storms can be extracted irrespectively of how calibrated are the TEC data used.

Reference

Baran L.W., I.I. Shagimuratov, N.J. Tepenitsina, 1997. The Use of GPS for Ionospheric Studies, Artificial Satellites, Vol.32, No 1, 49-60.

Baran L.W., I.I. Shagimuratov, 1998. The use of GPS for monitoring of the ionospheric disturbances, Advances in Positioning and References Frames, International Association of Geodesy Symposia, Springer, Vol. 118, Brunner, F.K. (Ed.), 252-258.

Baran L.W., I.I. Ephishov, I.I. Shagimuratov, 2001. Ionospheric Total Electron Content Behaviour During November 1997 Storm, Physics and Chemistry of the Earth (C), 26, 341-346.

Coco D.S., C. Coker, S.R. Dahlke, J.R. Clynch, 1991. Variability of GPS satellite differential group delay biases, IEEE Trans. Aerosp. Electron. Syst., 27, 931.

Forster M., A.A. Namgaladze, R.Y. Yurik, 1999. Thermospheric composition changes deduced from geomagnetic storm modeling, Geophysical Research Letters, 26, 16, 2625-2628.

Fuller-Rowell T.J., M.V. Codreson, H. Rishbeth, R.J. Moffett, S. Quegan, 1996. On the seasonal response of the thermosphere and ionosphere to geomagnetic storms, Journal of Geophysical Research, 101, 2343-2353.

Ho C.M., A.J. Manucci, U.J. Lindqwister, X. Pi, B.T. Tsurutani, 1996. Global ionosphere perturbations monitored by the worldwide GPS network, Geophysical Research Letters, 23, 22, 3219-3222.

Ho C.M., A.J. Manucci, X. Pi, , B.T. Tsurutani, L. Sparks, B.A. Iijima, B.D. Wilson, I. Harris, M.J. Reyes, 1998. Global ionosphere TEC variations January 10 1997 storm, Geophysical Research Letters, 25, 14, 2589-2592.

Jakowski N., S. Schlutter, E. Sardon, 1999. Total electron content of the ionosphere during geomagnetic storm on 10 January 1997, Journal of Atmospheric and Solar-Terrestrial Physics, 61, 299-307.

Krankowski A., L.W. Baran, I.I. Shagimuratov, 2002. Influence of the Northern Ionosphere on Positioning Precision, Physics and Chemistry of the Earth, 27, 391-395.

Krankowski A., L.W. Baran, I.I. Shagimuratov, 2005. Modeling and Forecasting of Total Electron Conten over Europe, Proceedings of Workshop&Symposium "Celebrating a Decade of the International GPS Service", Astronomical Institute of University of Berne, Berne, Switzerland.

Lastovicka J., 2002. Monitoring and forecasting of ionospheric space weather-effects of geomagnetic storms, Journal of Atmospheric and Solar-Terrestrial Physics, 64, 697-705.

Lu G., X. Pi, A.D. Richmond, R.G. Roble, 1998. Variations of Total Electron Content during geomagnetic disturbances: A model/observation comparison, Geophysical Research Letters, 25, 3, 253-256.

Lu G., A.D. Richmond, R.G. Roble, B.A. Emery, 2001. Coexistence of ionospheric positive and negative storm phases northern winter conditions. A case study, Journal of Geophysical Research, 106, 24495-24504.

Mannucci A.J., B.D. Wilson, D.N. Yuan, C.H. Ho, U.J. Lindqwister, T.F. Runge, 1998.

A global mapping technique for GPS-derived ionospheric total electron content measurements, Radio Science, 33, 3, 565-582.

Pi X., M. Mendillo, W.J. Hughes, M.J. Buonsanto, D.P. Sipler, J. Kelly, Q. Zhou, G. Lu, , T.J. Hughes, 2000. Dynamical effects of geomagnetic storms and substorms in the middle-latitude ionosphere: An observational campaign, Journal of Geophysical Research, 105, 7403-7417.

Prolss G.W., 1993. Common origin of positive ionospheric storms at middle latitudes and the geomagnetic activity effect at low latitudes, Journal of Geophysical Research, 98, 3981-3991.

Shagimuratov I.I., L.W. Baran, P. Wielgosz, G.A. Yakimova, 2002. The structure of Mid-and High-Latitude Ionosphere During September 1999 Storm Event Obtained from GPS Obserations, Annales Geophysicae, 20, 655-661.

Shiokawa K., Y. Ottsuka, T. Ogawa, K. Igarashai, S. Miyazaki, F.J. Rich, A. Saito, Y. Yumoto, 2000. Comprehensive imaging observations of midlatitude ionospheric disturbances during storm time substorms, Journal of Geophysical Research, 105, 27067-27080.

Tsagouri I., A. Belehaki, G. Moraitis, H. Mavromichalaki, 2000. Positive and negative ionospheric disturbances at middle latitudes during geomagnetic storms, Geophysical Research Letters, 27, 21, 3579-3582.

Wanninger L., 1993. The occurrance of ionospheric disturbances above Japan and

their effects on GPS positioning, Proceedings of the 8th International Symposium on Recent Crust Movemens (CRCM 93), Kobe, Japan, December 1993.

Wanninger L., E. Sardon, R. Warnant, 1994. Determination of the Total Electron Content with GPS - Difficulties and their Solution, Proceedings of the Beacon Satellite Symposium 1994, Alberystwyth, Wales, UK.

Werner S., G.W. Prolss, 1997. The position of the ionospheric trough as a function of local time and magnetic activity, Advances in Space Research, 20, 9, 1717-1722.

Wielgosz P., L.W. Baran, I.I. Shagimuratov, M.V. Aleshnikova, 2004. Latitudinal variations of TEC over Europe obtained using GPS observation, Annales Geophysicae, 22, 405-415.

Wilson B.D., A.J. Mannucci, 1993. Instrumental biases in ionospheric measurements derived from GPS data, Proceedings of the Institute of Navigation GPS-93, Inst. of Navig., Alexandria, p.1343.

Wilson B.D., A.J. Mannucci, C.D. Edwards, 1995. Subdaily northern hemisphere ionospheric maps using an extensive network of GPS receivers, Radio Science, 30, 3, 639-648.

Zarraoa N., E. Sardon, 1996. Test of GPS for permanent ionospheric TEC monitoring at high latitudes, Annales Geophysicae, 14, 11-19.

COMBINED ASSIMILATION OF GPS BASED TEC DATA FROM CHAMP AND SAC-C FOR IONOSPHERE/PLASMASPHERE IMAGING

S. Heise[1], N. Jakowski[2]

[1]GeoForschungsZentrum Potsdam, Dept. Geodesy & Remote Sensing, Telegrafenberg, D 14473 Potsdam, Germany, e-mail: heise@gfz-potsdam.de
[2]DLR, IKN, Kalkhorstweg 53, D 17235 Neustrelitz, Germany

Abstract. Space based GPS observations onboard LEO satellites provide a valuable new data source for ionospheric remote sensing. The paper deals with application of GPS navigation measurements from CHAMP and SAC-C for reconstruction of 3d electron density distributions of the upper ionosphere and plasmasphere by assimilation of link related TEC measurements into an initial model prediction. We describe data processing and retrieval technique. Reconstruction results for selected assimilation examples are presented. We validate our results with CHAMP Langmuir Probe data and compare reconstructions based on data from only one and from both satellites.

Key words: ionosphere, plasmasphere, CHAMP, SAC-C, GPS.

1. Introduction

Dual frequency GPS observations are well proved and widely used for ionospheric monitoring. Information on the link related total electron content (TEC) can easily be derived from differential GPS phase measurements due to the frequency dependent ionospheric impact on radio signals. Beside the well-established GPS ground receiver networks, the installed GPS receivers on board of LEO (Low Earth Orbiting) satellites like CHAMP and SAC-C provide a valuable data source for ionospheric remote sensing and tomography. Both the CHAMP and SAC-C satellites permanently track several GPS satellites using dedicated zenith looking antennas for precise orbit determination (Fig. 1). These 0.1 Hz sampled dual frequency navigation measurements provide valuable information on the ionization state of the upper ionosphere and plasmasphere up to GPS altitudes on a global scale. After preprocessing and calibration link related TEC measurements are derived from the GPS navigation observations. Three-dimensional electron density information for the upper ionosphere and plasmasphere is retrieved by assimilating these TEC data into the Parameterized Ionospheric Model (PIM).

In specific periods CHAMP and SAC-C circle the earth in nearly the same orbit plane due to their different orbit properties. We focus on these constellations, which are of special interest for the combined assimilation of

TEC measurements from both satellites.

In this paper we briefly describe data processing and retrieval technique for the reconstruction of ionospheric and plasmaspheric electron density distributions by assimilation of link related TEC measurements from CHAMP and SAC-C. Reconstruction results for selected assimilation examples are presented by means of two-dimensional slices along the respective CHAMP/SAC-C orbit plane. Using electron density measurements from the CHAMP Langmuir Probe we validate our reconstruction results along the CHAMP path and discuss the impact of the TEC measurements from SAC-C on the reconstruction result at CHAMP orbit altitudes.

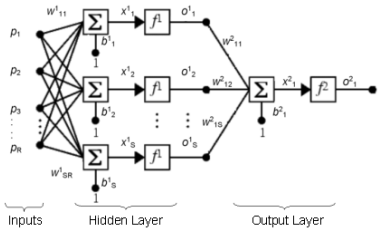

Fig. 1. Scenario of GPS navigation measurements onboard CHAMP and SAC-C.

2. Observation scenario and data processing

Both CHAMP and SAC-C circle the earth in nearly polar orbits tracking several GPS satellites using dedicated zenith looking antennas (Fig. 1). The orbit time differs slightly (about 93 and 97 minutes) due to the different altitudes of CHAMP (about 400 km) and SAC-C (about 700 km). But while the SAC-C orbit is sun synchronous and therefore fixed in local time, the CHAMP orbit plane moves slowly through all local time sectors. Thus, there are periods when both satellites circle the earth in nearly the same orbit plane but at different altitudes. These periods are of special interest for the combined assimilation of CHAMP/SAC-C TEC data. In this paper we focus on periods when the angles between both orbit planes were less than 15° (Fig. 2). The following days of 2002 have been selected accordingly for our investigations: 30-47, 163-176 and 293-309.

The processing system applied for this study represents a multi satellite

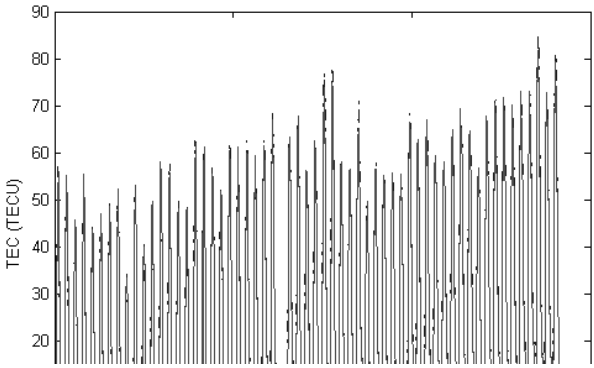

Fig. 2. Angle between CHAMP and SAC-C orbit plane for 2002.

extension of that which has originally been developed for the retrieval of 3-d electron density information using only CHAMP GPS data (e.g. Heise et al., 2002). The data processing basically consists of 3 parts (Fig.3): preprocessing, calibration and assimilation. Main inputs are CHAMP/SAC-C navigation measurements and orbit data from GPS and both LEO satellites. The preprocessing includes a GPS data quality check concerning outliers and cycle slips (according to Blewitt, 1990). Furthermore, we derive relative TEC from pseudorange-leveled differential carrier phases and allocate orbit information to each measured GPS transmitter - LEO receiver link. This link related TEC has to be calibrated for differential code biases (DCB) during the next processing step. A model assisted approach involving the known DCB of GPS is applied to estimate the DCB of CHAMP and SAC-C. Three-dimensional electron density information is retrieved by assimilating the integral TEC data into the Parameterized Ionospheric Model (PIM, Daniell et al., 1995).

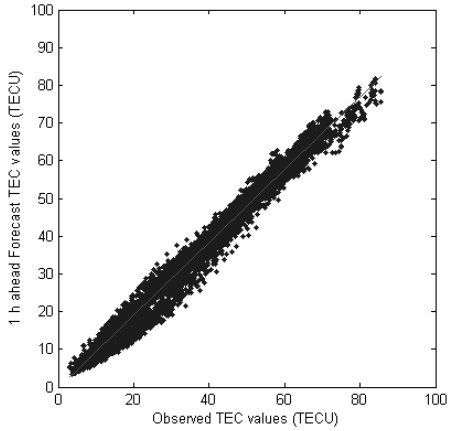

Fig. 3. Scheme of data flow and processing for reconstruction of electron density distributions from CHAMP and SAC-C GPS navigation measurements

3. Derivation and assimilation of GPS TEC data

To calculate the link related TEC we use differential GPS carrier (L1 - L2) and code (P2 - P1) phase measurements and work finally with pseudorange-leveled carrier phase differences. Absolute TEC values along the numerous radio links are estimated after calibrating the instrumental differential code biases (DCB) of each LEO receiver - GPS transmitter combination in a separate way. During this calibration procedure we estimate only the LEO DCBs and use the GPS DCBs from GPS ground station network bias solutions (e.g. Sardon, 1994). To estimate the LEO DCB (zenith antenna) a model assisted technique has been developed which takes advantage of the known GPS biases and comparatively low TEC above Low Earth Orbiter (LEO) altitudes in polar regions and during nighttime intervals. We assume a good average agreement between model and real ionization state under these conditions. Thus, LEO DCB is estimated by the average difference of (uncalibrated) link related TEC measurements and corresponding modelled TEC values. For assistance the Parameterized Ionospheric Model (PIM) is used. Applying this method we derived a reliable bias solution for the CHAMP receiver (Fig. 4, upper panel) varying within a spread RMS below 1 TECU for the year 2002. The SAC-C receiver DCB (Fig. 4, lower panel) could be derived comparatively stable.

The three dimensional electron density distribution is reconstructed by assimilating TEC measurements into the ionospheric/plasmaspheric model PIM which includes also the Gallagher model (Gallagher et al., 1988) of the plasmasphere. For this purpose, PIM is discretized on a global voxel structure

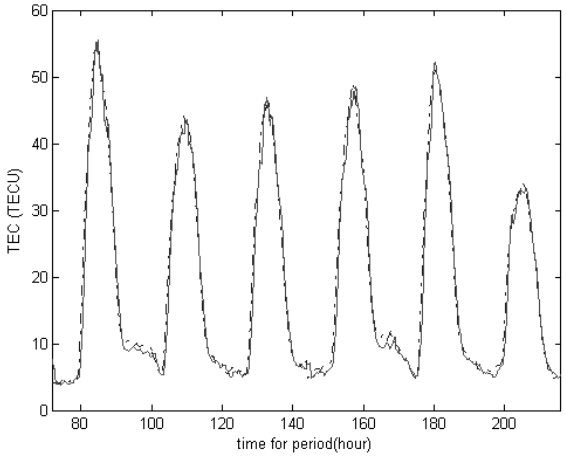

Fig. 4. Differential code bias estimation for the year 2002 concerning GPS navigation measurements onboard CHAMP (upper panel) and SAC-C (lower panel).

(Fig. 5) which covers the ionosphere and plasmasphere up to GPS altitudes. For each reconstruction we apply about 7000 CHAMP/SAC-C TEC measurements from 93-minute time intervals (one CHAMP revolution). The ionospheric/plasmaspheric system is considered to be stationary over this period. With respect to large scale changes in topside ionosphere/plasmasphere electron density distribution, this assumption appears applicable in most cases. The assimilation method is based on an iterative algorithm (e.g. Heise et al., 2002) which adapts the initial model assumption to the TEC measurements by applying multiplicative modifications, according to the widely used Multiplicative Algebraic Reconstruction Technique (MART, e.g. Kunitsyn et al., 2003). These modifications are determined by the ratio between the link related TEC measurements and the corresponding TEC values derived from the voxel structure after each iteration step. The validity of the resulting reconstruction depends of course on the data coverage and the initial model. Nevertheless, we obtain a physically reasonable reconstruction which represents at least an improvement over the initial model assumption.

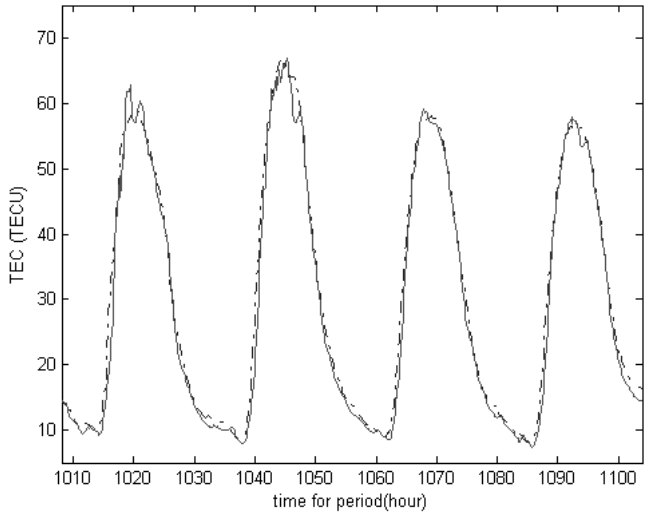

Fig. 5. Voxel structure (meridional slice) for assimilation of link related TEC data into an ionospheric model (e.g. PIM).

4. Results and validation

The assimilation result is a global 3-dimensional electron density distribution, covering the region between CHAMP and GPS orbit altitudes. The strongest assimilation impact is obviously found in the region near the CHAMP/SAC-C orbit plane while other areas of the voxel structure give the pure initial model, completely unaffected by the assimilation process. Thus, to present assimilation results we consider 2-dimensional slices with respect to the common CHAMP/SAC-C orbit plane. The left panel of Fig. 6 shows such a slice for a selected assimilation example and gives an impression of the reconstructed electron density distribution near the orbit plane (from around 22:30 LT in the East to 10:30 LT in the West). Beside the clear difference between day- and nighttime ionosphere and plasmasphere, Fig. 6 (left panel) reveals a considerably increased electron density in the nighttime northern hemisphere plasmapause region. This is also clearly visible in the right panel of Fig. 6 which shows the percentage deviation of the assimilation result from the initial model assumption. The remarkable deviation in the plasmapause region can be considered as an assimilation correction of the initial (PIM) plasmapause position. In this context it is interesting to compare the assimilation result shown in Fig. 6 with the corresponding reconstruction based on CHAMP TEC data only. This is shown in Fig. 7 (left panel) and reveals significant differences to the combined CHAMP/SAC-C reconstruction in the plasmasphere region. Fig. 7 (right panel) indicates that this difference is not caused by an absence of data coverage (given in link related TEC measurements per voxel). Thus, we could conclude that TEC data from SAC-C hold additional information on the plasmaspheric electron density distribution which are not covered by the CHAMP TEC measurements. This can be explained by the different orbit altitudes. While the integral TEC measurements from CHAMP are obviously dominated by the rather high electron densities of the lower topside ionosphere this is not the case for SAC-C which circles the earth far above the ionospheric electron peak densities. On the other hand, CHAMP and SAC-C data have not been measured at the same time (about 20 minutes time delay at 60° N, nighttime sector). Thus, the differences between pure CHAMP and combined CHAMP/SAC-C results could be caused by a rapid change in the plasmaspheric electron density distribution.

The in situ electron density measurements from the CHAMP Langmuir Probe (LP) provide a unique data source to validate the assimilation results along the CHAMP path and to investigate the impact of the SAC-C TEC data on the reconstruction result at CHAMP orbit altitudes. Of course these data are not sufficient to validate the entire reconstruction result. But systematic errors in the derived electron density along the CHAMP path allow the identification of general deficiencies resulting in systematic errors of the reconstructed electron density above the CHAMP orbit height. Fig. 8 shows comparisons between LP on the one hand and CHAMP/SAC-C assimilation, pure CHAMP assimilation and PIM on the other hand (left panel: global comparison and right panel: low latitudes only). The comparison between PIM, assimilation and LP reveals a significant improvement over the initial model by the assimilation. Nevertheless, it has to be noticed that the assimilation results tend to underestimate the in situ measurements. But Fig. 8 shows a noticeable improvement of the pure CHAMP assimilation by additional use of SAC-C data. Showing a similar RMS agreement, the mean absolute deviation (ΔABS) of the pure CHAMP reconstruction is significant-

ly higher than for the combined CHAMP/SAC-C assimilation. Furthermore, comparison between left and right panel of Fig. 8 reveals general difficulties in modeling the equatorial ionosphere.

Beside the comparisons along the CHAMP path, pure SAC-C reconstructions can be compared with corresponding CHAMP results and PIM to validate pure CHAMP assimilation results at SAC-C altitudes. Fig. 9 (left panel) reveals a much better agreement between SAC-C and CHAMP results than between SAC-C and PIM. Thus, the assimilation of CHAMP TEC data significantly improves the performance of the initial model at SAC-C orbit altitudes. On the other hand, Fig. 9 (right panel) shows the comparison of combined CHAMP/SAC-C reconstructions with corresponding pure CHAMP results and PIM along the SAC-C path. The differences between pure CHAMP and combined CHAMP/SAC-C assimilation reveal the impact of the SAC-C data.

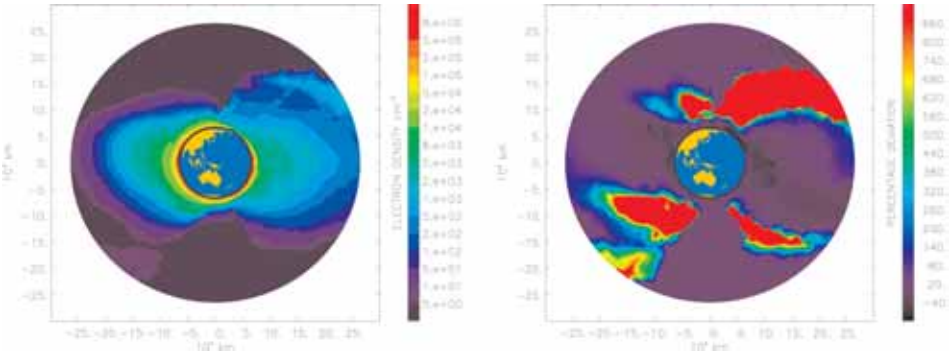

Fig. 6. Meridional slices in the CHAMP orbit plane (along 233° E, local time 22:30), assimilation example for October 27, 2002, Begin of assimilation: 06:13 UT, duration: 93 minutes. Left panel: Reconstruction of the ionospheric/plasmaspheric electron density distribution after the assimilation of TEC data from CHAMP and SAC-C (full CHAMP revolution). Right panel: Percentage deviation of the assimilation result from the initial model (PIM).

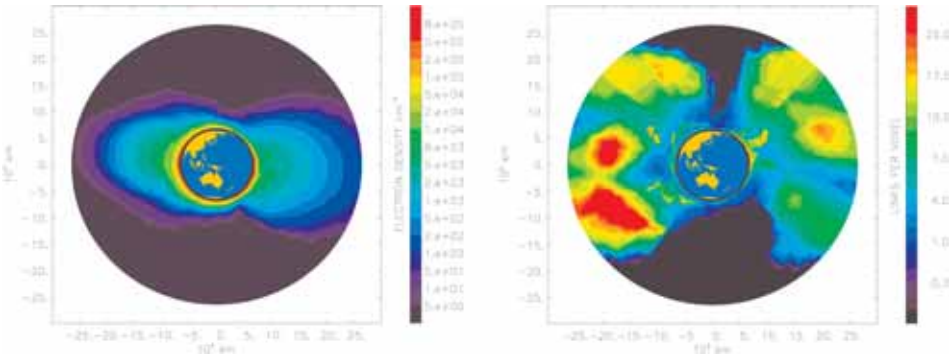

Fig. 7. Meridional slices in the CHAMP orbit plane, same assimilation example as shown in Fig. 6 but using only CHAMP TEC data. Left panel: Reconstruction of the ionospheric/plasmaspheric electron density distribution. Right panel: Corresponding data coverage

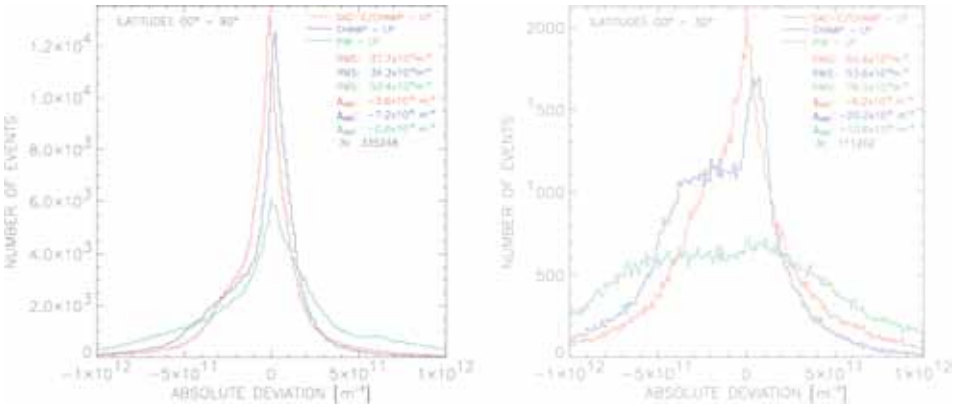

Fig. 8. Electron density comparisons for 2002, days of the year 36-47, 166-176, 293-309. Absolute deviations between CHAMP Langmuir Probe (LP) and: CHAMP/SAC-C assimilation, pure CHAMP assimilation and PIM. Left panel: global comparison. Right panel: low latitudes only (0° till 30° latitude, both hemispheres).

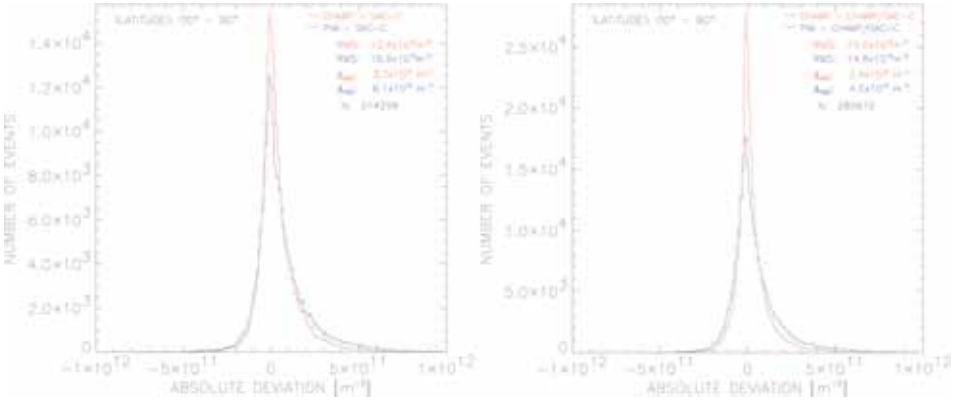

Fig. 9. Electron density comparisons along SAC-C path for 2002, days of the year 36-47, 166-176, 293-309. Left panel: Absolute deviation between pure CHAMP and SAC-C assimilation and between PIM and SAC-C assimilation. Right panel: Same as left panel but CHAMP/SAC-C in place of pure SAC-C assimilation.

5. **Conclusions**

GPS receivers on board LEO satellites are a powerful data source for imaging large scale structures of the ionosphere and plasmasphere on a global scale. The assimilation of link related TEC data from CHAMP and SAC-C provides an estimation of the electron density distributions of the upper ionosphere and plasmasphere. The validation with Langmuir Probe measurements indicates a noticeable improvement over pure CHAMP reconstruction results by the additional assimilation of link related TEC measurements from SAC-C. The comparison of pure SAC-C reconstructions with corresponding

CHAMP results and PIM shows significant improvements over the initial model at SAC-C orbit altitudes produced by the assimilation of CHAMP TEC data. Further improvement of assimilation results can be expected from additional link related TEC measurements (e.g. GRACE) and more accurate initial model assumptions.

Acknowledgments. The Authors are grateful to the teams of CHAMP and SAC-C and to the data providers GFZ/ISDC and JPL.

References

Blewitt, G., 1990. An automatic editing algorithm for GPS data. Geoph. Res. Letters, 17(3), 199-202.

Daniell, R.E., L.D. Brown, D.N. Anderson, M.W. Fox, P.H. Doherty, D.T. Decker, J.J. Sojka, R.W. Schunk, 1995. Parameterized ionospheric model: A global ionospheric parameterization based on first principles models. Radio Sci., 30, 1499-1510.

Gallagher, D.L., P.D. Craven, R.H. Comfort, 1988. An empirical model of the Earth's plasmasphere. Adv. Space Res., 8(8), (8)15-(8)24.

Heise, S., N. Jakowski, A. Wehrenpfennig, Ch. Reigber, H. Luhr, 2002. Sounding of the topside ionosphere/plasmasphere based on GPS measurements from CHAMP: Initial results. Geoph. Res. Letters, 29(14), 10.1029/2002GL014738.

Kunitsyn, V.E., E.D. Tereshchenko, 2003. Ionospheric Tomography. Springer, Berlin, Heidelberg, New York.

Sardon, E., A. Rius, N. Zarraoa, 1994. Estimation of the transmitter and receiver differential biases and the ionospheric total electron content from Global Positioning System observations. Radio Sci., 29(3), 577-586.

THE WITHIN THE HOUR VARIABILITY IN TEC: SOME PRELIMINARY RESULTS

K. V. Polimeris[1], V. Romano[2], S.S. Kouris[1] and B. Zolesi[2]

[1]Electrical and Computer Engineering Department., Aristotle University of Thessaloniki, GR-54124 Thessaloniki, Greece, email: luftfave@yahoo.com
[2]Istituto Nazionale di Geofisica e Vulcanologia, Via di Vigna Murata 605, 00143 Rome, Italy, email: romano@ingv.it

Abstract. Using 10-minutes TEC daily data measured at Matera (Italy) the within-the-hour variability in TEC is investigated. It is found that this type of variability is negligible except at sunrise and sometimes at sunset where it reaches values as 0.20 higher or lower over the corresponding standard hourly value.

Key words: Total Electron Content, ionospheric variability.

Introduction

Day-to-day and hour-to-hour variability are permanent features of the ionospheric F-region (Kouris and Fotiadis, 2002). Moreover, variations of the critical frequency foF2 in the time interval of an hour have been reported in different papers (Kouris et al., 2000; Fotiadis et al., 2001; Zolesi et al., 2001). In these papers it was pointed out that an ionospheric variability of about 10% in the time interval of an hour is always present. In Fig. 1 the deciles of variability in foF2 from hourly daily data and from measurements made every 10 minutes at Rome are reported. It is clear from this Figure that an estimation error of 10% to 20% and even higher might occur when predictions are based on hourly daily data.

In the present work we consider TEC data measured at Matera (Geographic Coordinates: 40.7° N; 16.6° E) every 10-minutes during the years 1996 to 2000 and also 5-minutes measurements of foF2 made at Rome (41.9° N; 12.5° E) during nearly the same period. To investigate the within-the-hour variability in TEC, the 10-minutes relative deviations (Fotiadis et al., 2001) in each time interval of an hour (half an hour before and after each exact hour) of each day/month/year are calculated using the expression:

$$dTEC = \frac{TEC_{10} - TEC}{TEC} \qquad (1)$$

where dTEC is the 10-minute relative deviation, TEC_{10} is the measured value of TEC every 10-minutes and TEC is the hourly daily measured value. A sim-

ilar expression is used to calculate the dfoF2 variability within-the-hour of foF2.

We want to note that there are used relative deviations in the interval of an hour with respect to the corresponding hourly daily value in order to remove the regular daily variation and to avoid any effect of the variability from hour-to-hour on the results of the analysis; thus consider the totality of relative deviations as a whole.

Results and discussion

This investigation points out that the within-the-hour variability in TEC has a different behaviour than that in foF2. It can be assumed that there is no essential variability in TEC in the time interval of an hour. This is clear from Fig.2 where the deciles (upper and lower) of the variability in TEC from hourly daily measurements and from measurements made every 10-minutes are reported. Comparison of Figs.1 and 2 shows clearly the difference. We have to note that the deciles have been counted from the relative deviations of the daily, hourly or 10-minutes measurements, respectively and are calculated accordingly using the expressions:

$$dTEC = \frac{TEC - TEC_m}{TEC_m} \qquad (2)$$

$$dTEc = \frac{TEC_{10} - TEC_{10m}}{TEC_{10m}} \qquad (3)$$

where TEC is the hourly daily value, TECm the corresponding monthly median, and TEC_{10} is the 10-min. daily value and TEC10m is the corresponding monthly median value.

Fig.3a shows the 10-minutes relative deviations calculated using eq.(1) from measurements made on the 4 and 14 December 1997. For comparison in Fig.3b the 10-min. relative deviations of foF2 of the same days are reported. It is evident that in the case of foF2 there is a substantial variability in the time interval of an hour whereas the within-the-hour variability in TEC is practically negligible apart during sunrise and sunset. It seems that these variations of dTEC in Fig.3a are simple due to the nearly linear increase or decrease of TEC during its diurnal normal variation, that is at sunrise and sunset; then the relative deviations may reach values up to around 0.20.

In Figs.4a and 4b there are illustrated similar plots of dTEC and dfoF2 and the same in Figs.5a and 5b. These plots confirm the above statement. We want to note that the variability in TEC is not always present during sunset. These preliminary results should be further confirmed, using more data. The behaviour of TEC during disturbed periods should also be studied.

Conclusions

The within-the-hour variability in foF2 is usually about 10% of the corresponding hourly daily value, except at sunrise and sunset or during disturbed periods where variability values such as 30 or 40% may be reached. On the contrary the within-the-hour variability in TEC is negligible, except at sunrise and often at sunset.

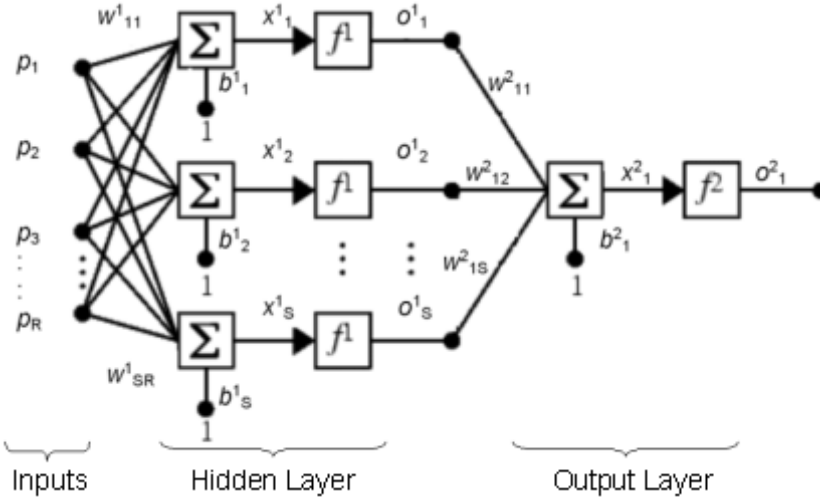

Fig. 1. Deciles of variability in foF2 (Rome) from hourly daily measurements (black) and from measurements every 10-minutes (red).

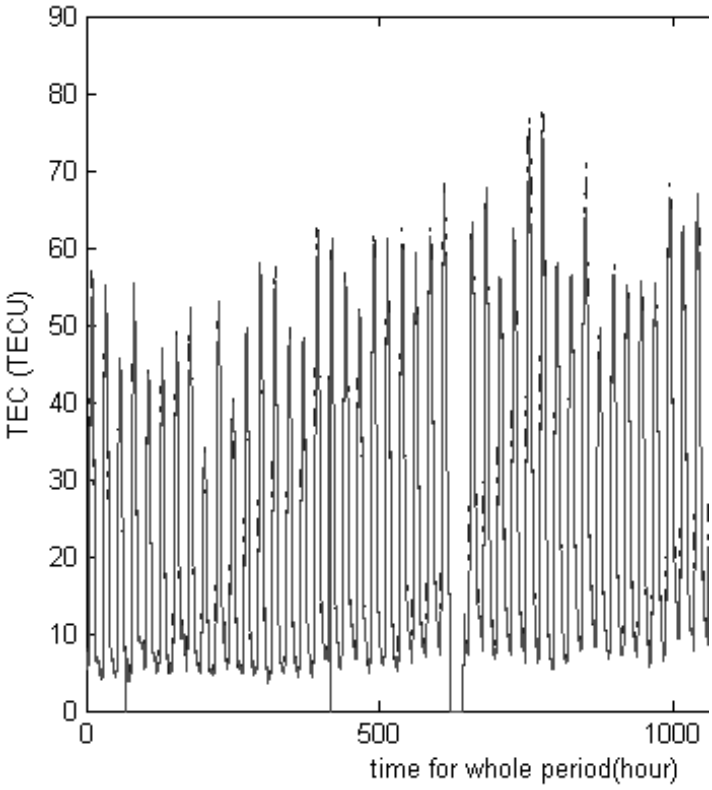

Fig. 2. Deciles of variability in TEC (Matera) from hourly daily data (black) and TEC-data measured every 10-minutes (red).

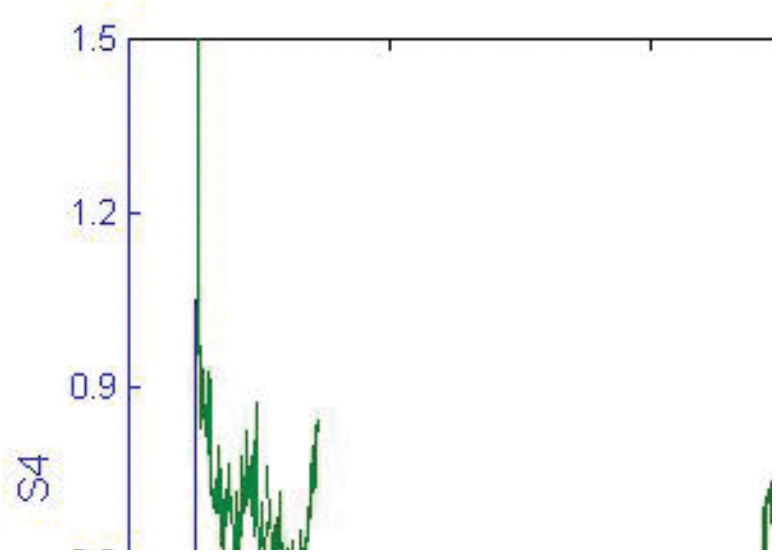

Fig. 3a. Variability within-the-hour of TEC from 10-min. measurements using eq. (1).

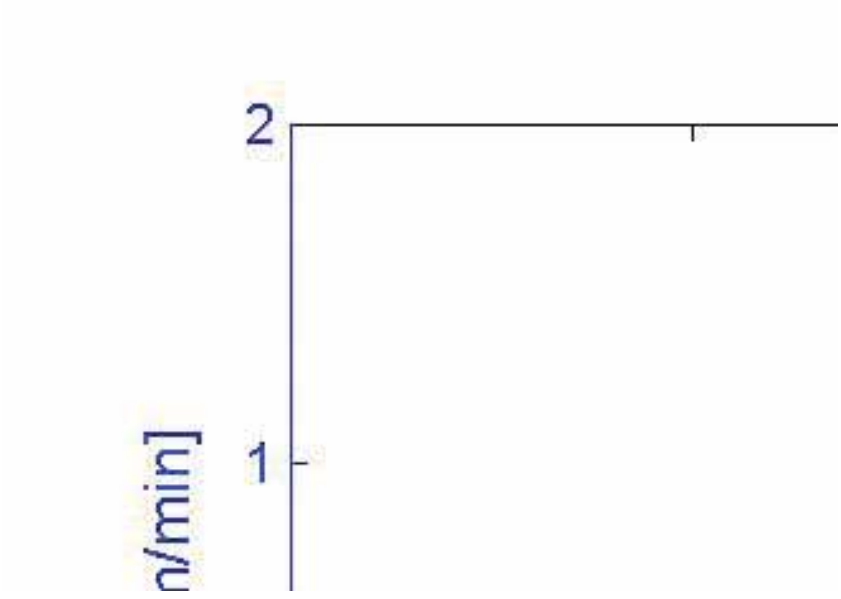

Fig. 3b. Variability within-the-hour of foF2 from 10-min. measurements.

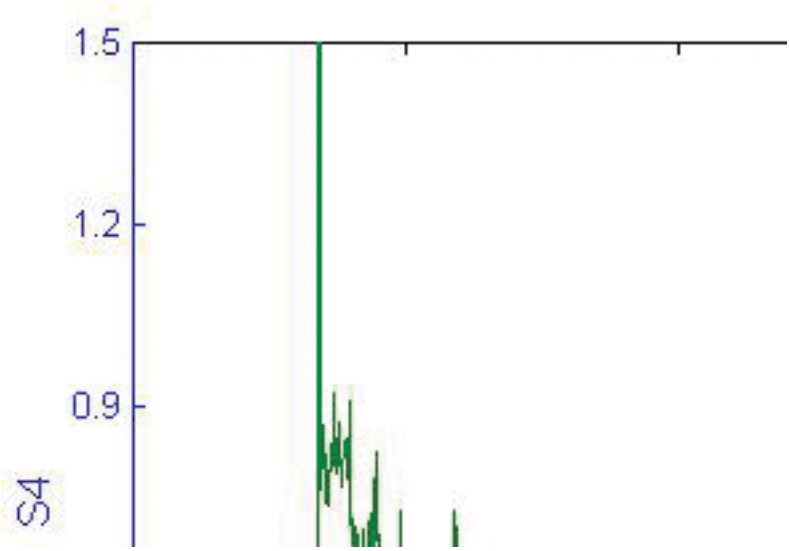

Fig.4a. Variability within-the-hour of TEC from 10-min. measurements using eq. (1).

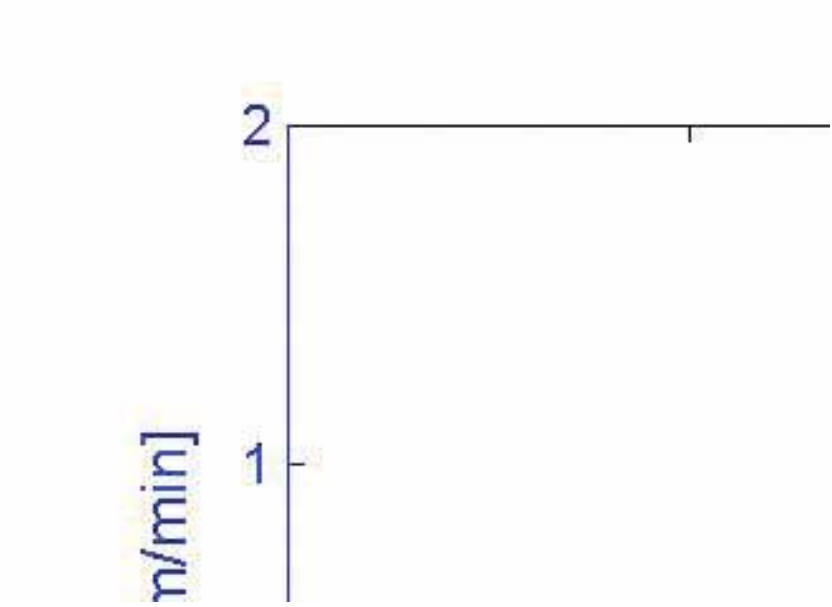

Fig. 4b. Variability within-the-hour of foF2 from 10-min. measurements.

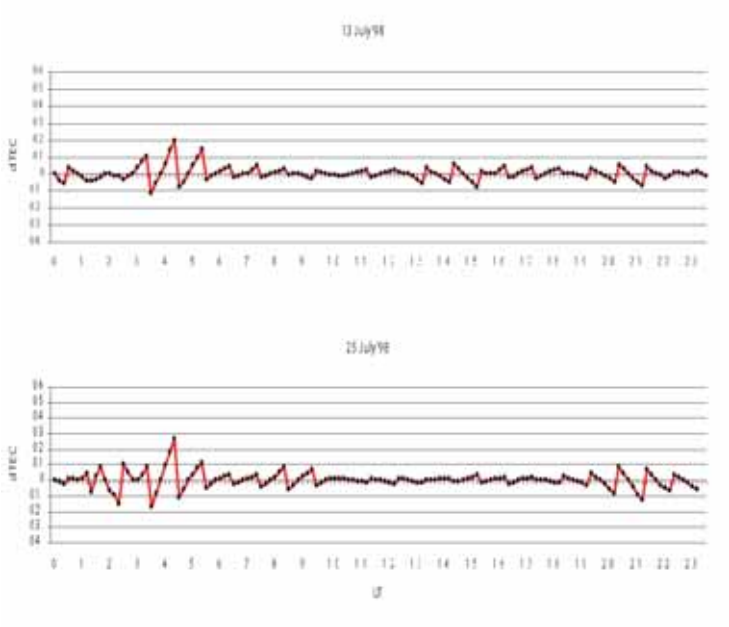

Fig.5a. Variability within-the-hour of TEC from 10-min. measurements using eq. (1).

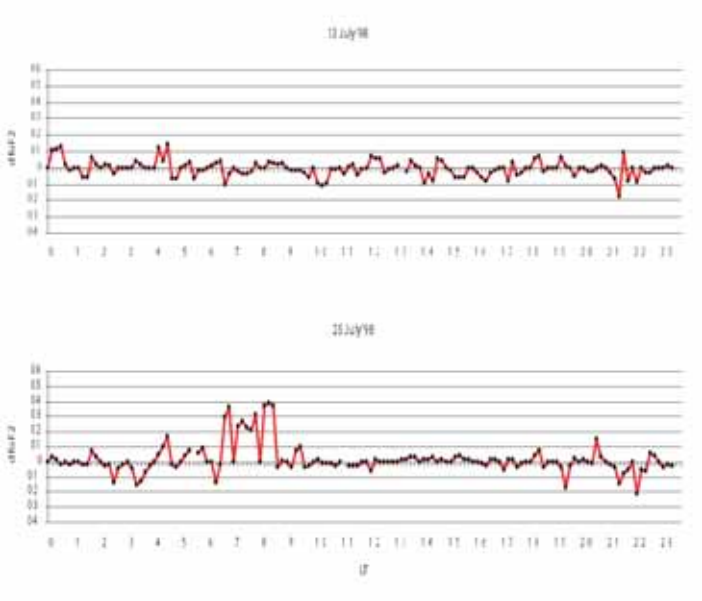

Fig.5b. Variability within-the-hour of foF2 from 10-min. measurements

Acknowledgements. This work is part of a joint Greek-Italian research project supported by the cultural collaboration (7th protocol) between the two countries.

6. References

Fotiadis D.N., S.S. Kouris and B. Zolesi, 2001, Preliminary results on the within-the-hour ionospheric variability, Phys. Chem. Earth (C), vol. 26(5), pp. 315-318.

Kouris S. S. and D. N. Fotiadis, 2002, Ionospheric variability : A comparative statistical study, Adv. Space Res. vol. 29(6), pp. 977-985.

Kouris S.S., B. Zolesi, D.N. Fotiadis and C. Bianchi, 2000, On the variability within-the-hour and from hour-to-hour of the F-region characteristics above Rome, Phys. Chem. Earth (C), vol. 25(4), pp. 347-351.

Zolesi B., S.S. Kouris, D.N. Fotiadis and C. Scotto, 2001, Evaluation of the ionospheric noise and variability within the hour by 5 minutes ionospheric soundings, Phys. Chem. Earth (C), vol. 26(5), pp. 359-362.

IONOSPHERIC SCINTILLATION OBSERVED DURING OCTOBER 2003 STORM

B. Forte

The Abdus Salam International Centre for Theoretical Physics, Strada Costiera 11, 34100, Trieste, Italy, e-mail: bforte@ictp.it

Abstract. Rapid fluctuations in the amplitude and phase of radio waves propagating through the ionosphere may be caused by small-scale plasma density irregularities. Ionospheric scintillation events have been observed on signals from GPS satellites during successive phases of October 2003 storm. Those observations have been made by means of a commercial single frequency GPS receiver, suitably operated in order to carry out the measurements of those fluctuations caused by small-scale electron density irregularities. The relationship between scintillation and TEC fluctuations is also investigated by means of dual frequency data from a close geodetic receiver. Structures of enhanced electron density have been observed during occurrence of scintillation and high TEC fluctuations events. Phase scintillation is characterized by means of a recently new proposed estimator, which provides a more robust information than classical phase scintillation index against data detrending effects.

Key words: radiowaves scintillation, TEC fluctuations, GPS scintillation monitors, auroral oval, magnetic storm.

1. Introduction

Experimental measurements over the last 3 decades have shown that plasma irregularities producing transionospheric signal fading are mainly located at F layer heights. The irregularities are located mainly at altitudes between 250 and 500 km, with peak of occurrence around 400±50 km of altitude. In-situ measurements have also shown the possibility of irregularities existing at altitudes of 1000 km as well as at E layer heights (Aarons, 1982).

Boundary and auroral blobs have been observed inside or on the equatorward edge of the auroral ova (Tsunoda, 19888; Vickrey et al., 1980). Auroral blobs seem to be produced by non-uniform particle precipitation in the auroral oval, while boundary blobs seem to be locally created but patches convecting through the nightside auroral oval and around toward the dusk (Robinson, 1985). Small scale plasma density features travel and form embedded into these large scale plasma density irregularities; they are able to produce scintillation on radio waves propagating through the ionospheric medium (Basu et al., 1985; Aarons and Allen, 1971; Martin and Aarons, 1977; Kersley et al., 1988a; Kersley et al., 1989; Kersley et al., 1988b; Pryse

et al., 1996).

An irregularity oval is usually associated with the auroral oval. Such an irregularity oval takes into account the region of plasma irregularities onset and it is a modification of the auroral oval with the irregularity oval presenting an intensity or strength parameter describing the irregularities. Both the auroral and irregularity ovals expand equatorward and polarward with increasing magnetic activity. The irregularity oval shrinks in intensity and area, and moves to high latitudes during long periods of both low and magnetic activity and low solar flux (Aarons and Kersley, 1995; Aarons, 1997). The small scale electron density irregularities forming in the irregularity oval can be responsible for radio wave scintillation even at L-band.

GPS scintillation monitors represent a suitable tool for monitoring ionospheric scintillations occurring on GPS satellites signals (Van Dierendonck et al., 1993; Beach and Kintner, 1999; Ganguly et al., 2004). On the basis of the results achieved by measurements conducted by using the Ionospheric Scintillation Monitor (ISM) (Van Dierendonck et al., 1993), it is a common and accepted opinion the fact that at high latitudes, GPS scintillation monitors (and consequently GPS receivers) observe high phase scintillation in presence of low intensity scintillation (Doherty et al., 2000; Pi et al., 2001). This is actually in contrast with what is expected at auroral latitudes on the basis of beacon polar orbiting scintillation indices, due to field-aligned sheet-like plasma density irregularities (Rino and Matthew, 1980). This is also in contrast with what it is expected at auroral latitudes for GPS ray paths and scintillation indices measured through GPS signals, where there is no clear and generic control of scintillation indices, due to the fact that the GPS ray paths alignement with L-shell seem difficult to occur (Forte and Radicella, 2004).

An explanation to sistematic observation of high phase scintillation against low intensity scintillation at high latitudes through commercial GPS scintillation monitors, has been provided on the basis of erroneous raw data detrending, characterized by fixed boundary conditions not suitable for tracking the actual ground diffraction pattern (Forte and Radicella, 2002).

The measurements presented here have been carried out by means of an independent commercial GPS receiver and scintillation activity has been characterized by means of typical S4 index and a new estimator for phase scintillation. The results clearly show the ability of such a technique of tracking saturating levels of scintillation both in phase and intensity, in contrast with accepted opinion in the community, e.g. (Doherty et al., 2000).

2. The experiment

A single frequency JNS100 Javad receiver has been used in order to measure raw data from GPS signals. The receiver has 50 channels, all in view: it is able to track L1 GPS signals, INMARSAT signals, SBAS corrections and GLONASS satellites, as well. It is characterized by low signal power tracking (down to 30 dB-Hz) fast acquisition and re-acquisition, up to 30 g's dynamic, advanced multipath mitigation, 10 cm code phase and 0.1 mm carrier phase precision in differential modes. It is connected to a normal PC by means of four high speed (115.2 Kbps) standard RS232 serial ports. It allows to record satellite positions, receiver position, C/A code pseudorange, L1 carrier phase,

Doppler, and C/N_o at sampling rates up to 100 Hz.

The experiment has been installed at the Sodankyla Geophysical Observatory (University of Oulu) and it is running since June 2003. The antenna has been placed on top of a tower 10 m tall, in order to avoid as much as possible, multipath from the ground or from obstacles on the ground. An elevation mask of 10º is also applied to the measurements as an additional protection against ground multipath. Raw L1 carrier phase and C/N_o are recorded at 20 Hz sampling rate. For the particular observation site this was a good tradeoff between data storage capability and spectral resolution of the phenomena under investigation. In the present experiment it has been observed that a higher sampling rate was redundant, because the noise level is reached at a Nyquist frequency of 10 Hz, already.

The scintillation indices presented here have been computed after a raw data detrending based on a 0.3 Hz cut-off frequency. This value and a fixed detrending boundary condition do not affect S_4 and the new phase scintillation estimator index (Forte, 2005). The new phase scintillation estimator is defined as the 1-min. standard deviation of phase rate of change, given by:

$$S_\phi = \sqrt{\left\langle \left(\frac{\partial \phi}{\partial t} \right)^2 \right\rangle} \tag{1}$$

where ϕ is the detrended phase component at high fluctuations frequencies, and $\eth\phi / \eth t$ has zero mean.

S_4 is defined as (Briggs and Parkin, 1963):

$$S_4 = \frac{< I^2 > - < I >^2}{< I >^2} \tag{2}$$

where I is the signal strength indicator and <.> denotes mean values. The signal strength indicator used in the present experiment is the signal-to-noise density in ratio-Hz S/N_o ($C/N_o = 10 \log \{S/N_o\}$) (Forte, 2005). The S_4 values are also corrected for ambient noise.

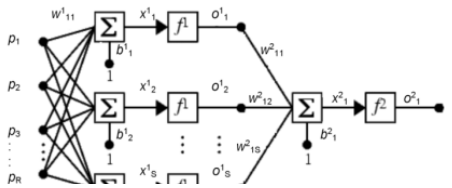

Fig. 1. Dst index during October 2003, as released by Kyoto University

Results and Discussion

The data presented here have been collected during the severe storm occurred at the end of October 2003. That event was characterized by a solar flare on 28-Oct.-2003, around 11 UT, which enhanced ionization levels in the daytime sector. Then, perturbations on the magnetic field developed leading to *Dst* index decreasing, up to -400 nT (Fig. 1). The main phase occurred on October 29, with a successive magnetic perturbation occurred in the first recovery phase, due to a new strong particle precipitation event.

At auroral latitudes, the onset of patchy structures with small scale electron density fluctuations has been observed essentially during the night between October 30 and 31. Some of those structures seem to be created locally by particle precipitation, while others have travelled in an antisunward direction through the polar cap.

Fig. 2 shows a particular case referring to PRN03 being tracked during 30-Oct.-2003, during different time intervals. Fig. 2a shows scintillation

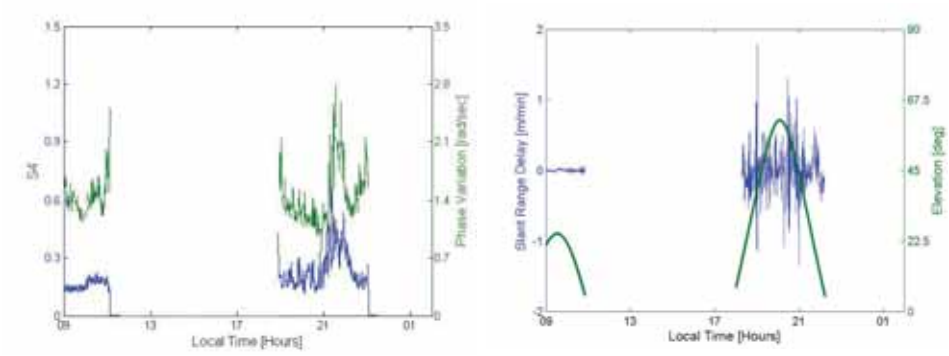

Fig. 2. (a) S_4 scintillation index (blue curve) and S_ϕ phase scintillation index (i.e., phase variation) in rad/sec (green curve) for PRN03, during 30-Oct.-2003; (b) TEC f;luctuations in L1 range equivalent (blue curve) in m/min and elevation angle (green dots) for PRN03, during 30-Oct.-2003.

indices: blue curve for S_4 index and green curve for the new phase scintillation estimator in rad/sec. Fig. 2b shows Total Electron Content (TEC) fluctuations in L1 range equivalent (m/min) and elevation angle for PRN03. Increasing of scintillation activity is observed around 21 LT in presence of TEC fluctuations enhancement (from 0.5 to 1.3 m/min, in absolute values), while elevation angle exceeds 65^o . This is a typical case of small scale irregularities embedded into larger scale features and traveling with them. S_4 values around 0.7 (strong scintillation regime) and S_ϕ up to 2.8 rad/sec imply the presence of strong electron density fluctuations, corresponding to the patchy structure traveling above the observing site during those hours.

Another case of interest is shown in Fig. 3. Fig. 3a shows scintillation indices S_4 and S_ϕ for PRN15, while Fig. 3b shows TEC fluctuations and elevation angles for the same satellite. Again, scintillation activity increasing (S_4

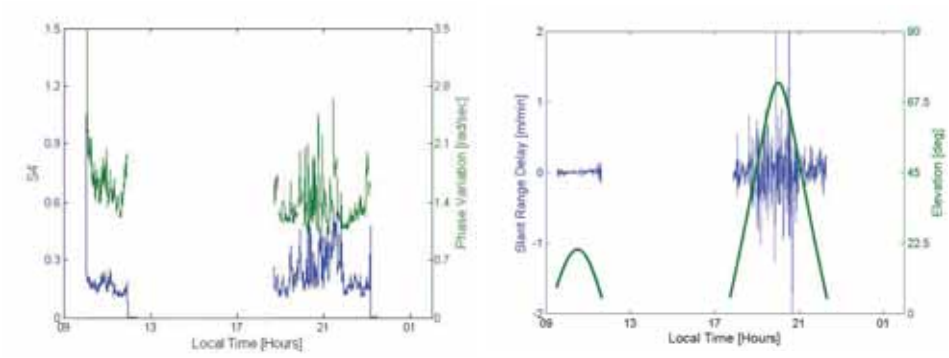

Fig. 3. (a) S_4 scintillation index (blue curve) and S_ϕ phase scintillation index (i.e., phase variation) in rad/sec (green curve) for PRN15, during 30-Oct.-2003; (b) TEC f;luctuations in L1 range equivalent (blue curve) in m/min and elevation angle (green dots) for PRN03, during 30-Oct.-2003.

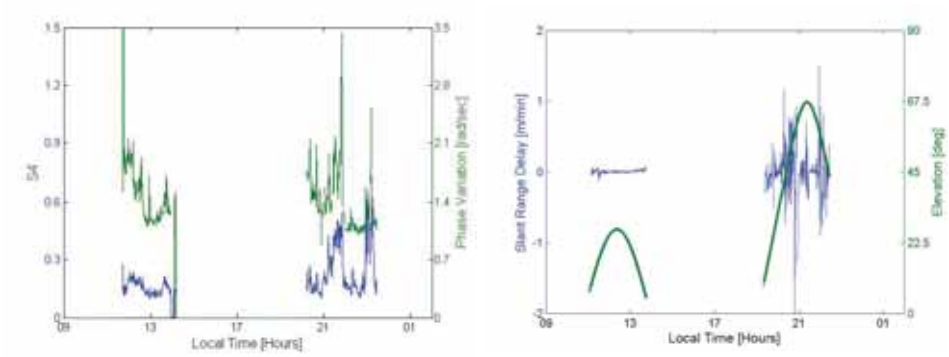

Fig. 4. (a) S_4 scintillation index (blue curve) and S_ϕ phase scintillation index (i.e., phase variation) in rad/sec (green curve) for PRN23, during 30-Oct.-2003; (b) TEC f;luctuations in L1 range equivalent (blue curve) in m/min and elevation angle (green dots) for PRN03, during 30-Oct.-2003.

up to 0.6 and S_ϕ up to 2.8 rad/sec) corresponds to TEC fluctuations enhancements (up to 1.5 m/min). The structures observed in Fig. 2 and 3 seem very similar and probably is the same structure being traversed by PRN03 and PRN15 ray paths from a common azimuthal sector.

Another satellite observing the same structure, but in a different way, is shown in Fig. 4. Here, scintillation indices and TEC fluctuations seem to indicate a clear transition from strong to weak and again to strong electron density perturbations, during the transit of satellite PRN23.

The cases shown by Fig. 2, 3, and 4 are just representative cases among those observed during that event at the observing site of Sodankyla. Contrary to what is expected from the literature, there is no evidence of "phase without amplitude" scintillation events. Scintillation activity enhancement is observed on both intensity scintillation index S_4 and "new" phase scintillation index S_ϕ, which are able to capture small scale plasma density irregularities effects on L band spread spectrum signals, like those broadcast by GPS satellites.

The effect of erroneous data detrending, responsible for high phase scintillation against low intensity scintillation at high latitudes, specially when using ISM equipment (Van Dierendock et al., 1993), seems not appearing in the present experiment. Such an effect has been overcome by using S_4 and S_ϕ as scintillation indices, which are not critically sensitive to detrending boundary conditions, like the classical phase scintillation index σ_ϕ (i.e., 1-min. standard deviation of high frequency component of received phase) (Forte, 2004).

It should be noted that the receiver used in such an experiment did not lose the signal even when measuring strong to saturating scintillation events. This confirms that the equipment used is suitable for tracking strong events, while widely deployed ISMs seems to be not able to observe S_4 values above $0.3 \div 0.4$, e.g. (Doherty, 2000).

3. Conclusions

Ionospheric scintillation measurements have been performed at an auroral observing site like Sodankyla, Northern Europe. Scintillation activity at L band has been monitored during the magnetic storm occurred at the end of October 2003, by using radio signals broadcast by GPS satellites. Scintillation activity has been characterized by the usual intensity scintillation index S_4 and by a suggested new phase scintillation index S_ϕ. The choice is due to the fact that both S_4 and S_ϕ seem relatively unaffected by detrending boundary conditions. When using S_4 and classical σ_ϕ, indeed, fixed detrending boundary conditions lead to misleading data interpretation, as it happens with ISMs which measure, somehow sistematically, high phase scintillation with low intensity scintillation at high latitudes.

Small scale plasma density fluctuations, able to produce radio wave scintillation at L band, have been observed mainly during the night between October 30 and 31, in the European nocturnal oval. These small scale electron density irregularities seem to be embedded within larger scale structures and to travel with them, since an increase of scintillation activity always corresponds to TEC fluctuations enhancements.

Those large scale features are probably produced both locally and traveled across the polar cap. The experimental equipment used here seems to be suitable for tracking strong scintillation regimes, since it does not show any loss of lock, even in presence of strong to saturating S_4 values.

4. References

Aarons J., and R.S. Allen, Scintillation boundary during quiet and disturbed magnetic conditions, J. Geophys. Res., vol. 76, N. 1, 1971.

Aarons J., Global morpholgy of ionospheric scintillations, Proc. IEEE, vol.70, N. 4, pp 360-378, 1982.

Aarons J. and L. Kersley, The sunspot cycle and auroral F-layer irregularities, Radio Sci, vol. 30, pp. 631-638, 1995.

Aarons J., Global Positionig System phase fluctuations at auroral latitudes, J. Atmosph. Terr. Phys., vol. 102, N. 48, pp.17219-17231, 1997.

Basu Su., S. Basu, and E. Mackenzie, Morphology of phase and intensity scintillations in the auroral oval and polar cap, Radio Sci., vol. 20, N. 3. pp. 347-356, 1985.

Beach T. L. and Kintner P. M., Simultaneous GPS observations of equatorial scintillations and total electron content fluctuations, J. Geophys. Res., Vol. 104, N. A10, pp. 22553-22565, 1999.

Briggs B. H. and Parkin I. A., On the variation of radio star and satellite scintillations with zenith angle, J. Atmos. Terr. Phys., Vol. 25, pp. 339-365, 1963.

Doherty H. P., S. H. Delay, C. E. Valladares, and J. A. Klobuchar, Ionosph. scintillation effects in the equatorial and auroral regions, Proc. ION-GPS-200, The Inst. of Navigation, Salt Lake City, 2000.

Forte B. and S.M. Radicella, Problems in data treatment for ionospheric scintillation measurements, Vol. 37, N. 6, 1096, doi:10.1029/2001RS002508, 2002.

Forte B. and S.M. Radicella, Geometrical control of scintillation indices: what happens for GPS satellites, Radio Sci., RS5014, doi: 10.1029/2002 RS002852, 2004.

Forte B., Optimum detrending for raw GPS data for scintillation measurements at auroral latitudes, J. Atmos. Sol.-Terr. Phys., under publication, 2005.

Ganguly S., Jovancevic A., Brown A., Kirchner M., Zigic S., Beach T. L., Groves K. M., Ionospheric scintillation monitoring and mitigation using a software GPS receiver, Radio Sci., Vol. 39, RS1S21, doi:10.1029/2002 RS002812.

Kersley L., S. E. Pryse, and N. S. Wheadon, Amplitude and phase scintillation at high latitudes over northern Europe, Radio Sci., vol. 23, N. 3, pp. 320-330, 1988a.

Kersley L., S. E. Pryse, and N. S. Wheadon, Small scale irregularities associated with a high latitude electron density gradient: scintillation and EISCAT observations, J. Atmosph. Terr. Phys., vol. 50, N. 6, pp. 557-563, 1988b.

Kersley L., C. D. Russell and S. E. Pryse, Scintillation and EISCAT investigations of gradient-drift irregularities inthe high latitude ionosphere, J. Atmosph. Terr. Phys., vol. 51, N. 4, pp. 241-247,1989.

Martin E. and Aarons J., F-layer scintillations and the aurora. J. Geophys. Res., vol 82, N. 19, 1977.

Pi X., Boulat B., Mannucci A. J., Reyes M., Sowers D., Ionospheric scintillations measured using GPS receivers during the current solar maximum, International Beacon Satellite Symposium, Boston, 2001.

Pryse S. E., Kersley L., and Walker I.K., Blobs and irregularities in the auroral ionosphere, J. Atmosph. Terr. Phys., vol. 58, N 1-4, pp. 205-215,1996.

Rino C.L. and S.J. Matthew, On the morphology of auroral zone radiowave scintillation, J. Geophys. Res., vol. 85, pp. 4139-4151, 1980.

Robinson, R. M., Sources of F region ionization enhancementes in the nighttime auroral zone, J. Geophys. Res., vol. 90, p. 7533, 1985.

Tsunoda, R. T., High-latitude F region irregularities: A review and synthesis, Rev. Geophys., vol. 26, p.719, 1988.

Van Drerendock A. J., J. A. Klobuchar, and Q. Hua, Ionospheric scintillation monitoring using a commercial single frequency C/A code receivers, Proc. ION-GPS-93, 1333, Inst. of Navigation, Arlington, VA, 1993.

Vickrey J. F., C. L. Rino and T. A. Potemra, Chatanika/TRIAD observations of unstable ionization enhancements in the auroral F-region, Geophys. Res. Lett., vol. 7, N. 10, pp. 789, 792, 1980.

THE NEW AIS-INGV IONOSONDE AT ITALIAN ANTARCTIC OBSERVATORY

V. Romano[1], J. B. Arokiasamy[2], F. Doumaz[1], M. Pezzopane1, U. Sciacca[1] and E. Zuccheretti[1]

[1]Istituto Nazionale di Geofisica e Vulcanologia, Rome, Italy, e-mail: ionoinfo@ingv.it
[2]TRIL-International Centre for Theoretical Physics, Trieste, Italy

Abstract. The Italian Ionospheric Antarctic Observatory of Terra Nova Bay (74.70S, 164.11E) was recently equipped with the AIS-INGV ionosonde developed at the Istituto Nazionale di Geofisica e Vulcanologia (INGV), Rome, (Italy). This paper aims to describe briefly which are the main characteristics of the instrument and show the good quality and reliability of the recorded ionograms.

Key words: ionosonde, antarctic ionospheric observatory, ionospheric data, vertical soundings.

1. Introduction

AIS-INGV (Advanced Ionospheric Sounder) is the digital low-power pulse-compressed ionosonde recently developed at the Istituto Nazionale di Geofisica e Vulcanologia (INGV), Rome, (Italy). The advanced HF-radar techniques employed permit the reduction of the transmitted power, weight, size, power consumption, hardware complexity and to have an excellent reliability.

Fig.1. Geographical location of the Italian Antarctic Base

This ionosonde was installed at the Italian Ionospheric Antarctic Observatory of Terra Nova Bay (74.70°S, 164.11°E) (Fig. 1).

In spite of the hard environmental conditions the ionosonde is capable of working without human intervention: sounding scheduling, device settings and data management are controlled remotely. For Space Weather applications the new ionosonde will continue to contribute to ionospheric data bases at high latitudes, with great improvement with respect to the past as for the on-line data availability, remote control and sounding reliability. In this work the new features of the Ionospheric Observatory are presented and the first results (ionograms and characteristics) are briefly discussed.

2. Main characteristics of the AIS-INGV

The aim of this new digital ionosonde (AIS-INGV) is to fulfill the request to have a simple and easy system to sound the ionosphere. To do this we designed a system in which the most advanced HF radar techniques have been employed (Skolnik, 1981; Skolnik,1990).

The result is the reduction of the transmitted power and, consequently, weight, size, power consumption and hardware complexity. These aims are appreciable in a harsh environment where a large amount of energy is not available at low cost. Nevertheless using low power techniques implies a large number of integrations which might be affected by quickly varying ionospheric conditions typical at high latitudes.

To compensate the power reduction a 16 bit complementary phase code is employed (Golay, 1961) together with pulse-compression and a phase coherent integration, giving the possibility to investigate the ionosphere with a power of 200W only. The ionosonde is completely programmable and the data acquisition, control, storage and on-line processing are supported by a PC (Zuccheretti et al., 2003; Bianchi et al., 2003; Arokiasamy et al., 2002).

3. Installation and configuration

Since 1991, the Italian Antarctic Observatory at Mario Zucchelli Station (MZS) has run hourly soundings during the austral summer. In 1995 observations were extended to the whole year, even though it is always difficult to obtain long and complete data series in such hard environmental conditions.

At the end of 2003 the analog IPS42 ionosonde was substituted by the new AIS-INGV digital ionosonde.

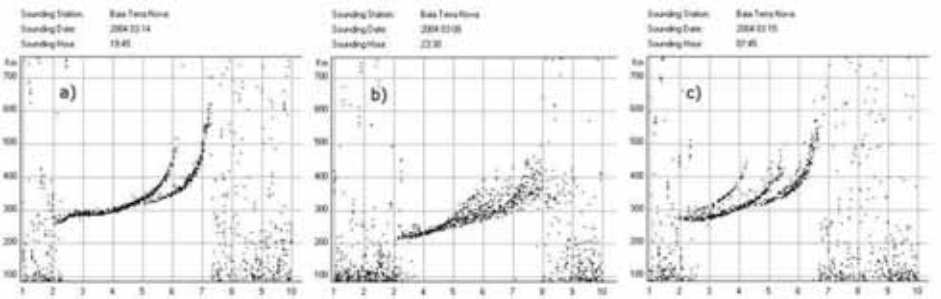

Fig.2. Three examples of soundings with a good quality of the trace. a) Ionogram in which the ordinary and the extraordinary rays are clearly visible. b) Ionogram characterized by spread-F echoes. c) Triple splitting of the trace (Z ray, ordinary and extraordinary rays) which can often distinguish ionograms recorded at high latitudes.)

In Fig. 2 three examples of good quality ionogram recorded by AIS-INGV are shown.

Like other recent ionospheric sounders, the AIS-INGV ionosonde is built around a Personal Compuetr (PC), which comprises the most important part. This allows the system to send ionograms through the Internet and makes remote control possible.

To better understand the problems and solutions for a such remote station it is important to review the organization of the observatory. The

Fig.3. The Italian Antarctic ionospheric observatory.

ionosonde and its PC are stored in a small container close to the antennas and distant from the populated base, MZS (Fig. 3).

In particular the ionosonde PC is connected through an HDSL (High bit rate Digital Subscriber Line) to the MZS local network, which is linked to the world via satellite link (Fig. 4). As a consequence data can be automatically sent to a server that makes ionograms available on demand by INGV where data are scaled and results are spread worldwide.

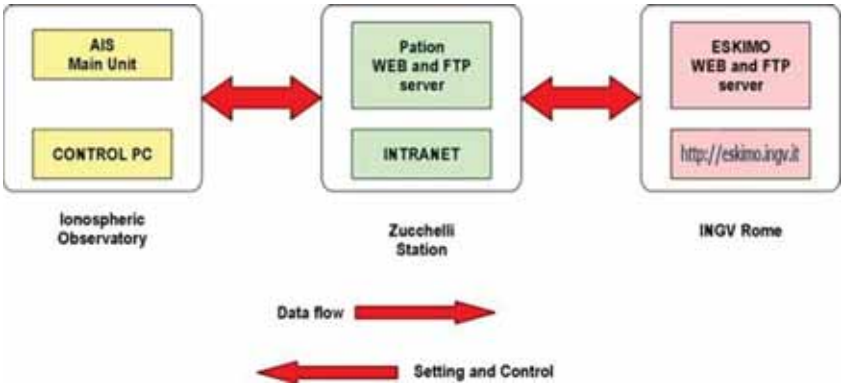

Fig.4. Diagram showing the AIS-INGV ionosonde data flow.

4. **First statistical analysis**

After installing the system a lot of work was spent determining the optimum operational parameters for the system. Particularly sensitivity; the number of integrations and the noise rejection filters were adjusted according to the local Antarctic environment. Good settings are confirmed by the quality of observed ionograms. We have considered 3401 ionograms acquired in about 130 days from 7th November 2003 to 29th March 2004. A simple statistical analysis was performed to confirm the correct operation of the instrument. In particular we divided the total number of ionograms into three categories: good quality ionograms in which exact parameters can be derived; poor quality ionograms in which it is necessary to add auxiliary letters to the scaled value and soundings without any kind of trace. In this last category blank ionograms are due to ionospheric absorption, as was confirmed by reference to other nearby ionospheric observatories (Scott Base and Casey).

The results are shown in Fig. 5 in which more than 70% of total number of ionograms collected were good quality ionograms and only 8% of cases are due to poor system sensitivity.

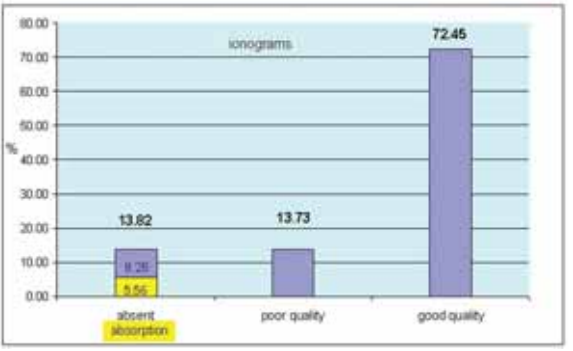

Fig.5. Simple statistical analysis of the ionogram quality.

5. A good agreement between different instruments

The presence of different instruments dealing with the ionosphere at the Antarctic observatory offers the possibility of validating results from one instrument with data coming from another.

One such case is the absence of ionograms due either to ionospheric absorption or to an improper working of the ionosonde. Variation from a normal behaviour can be due to the ionospheric absorption (Hunsucker, 1991). Two riometers have been installed at MZS since 1993. The riometer is a well-known instrument able to measure the relative opacity of the ionosphere (Romano et al., 2002).

In Fig. 6 the complete sequence of ionograms for 26th February 2004 is shown for two ionospheric absorption events.

At that time two ionosonde soundings per hour were performed, at minute 0 and minute 30, having a total number of 48 ionograms for each day.

The correspondence between the ionograms showing missing echoes and the absorption events is clear.

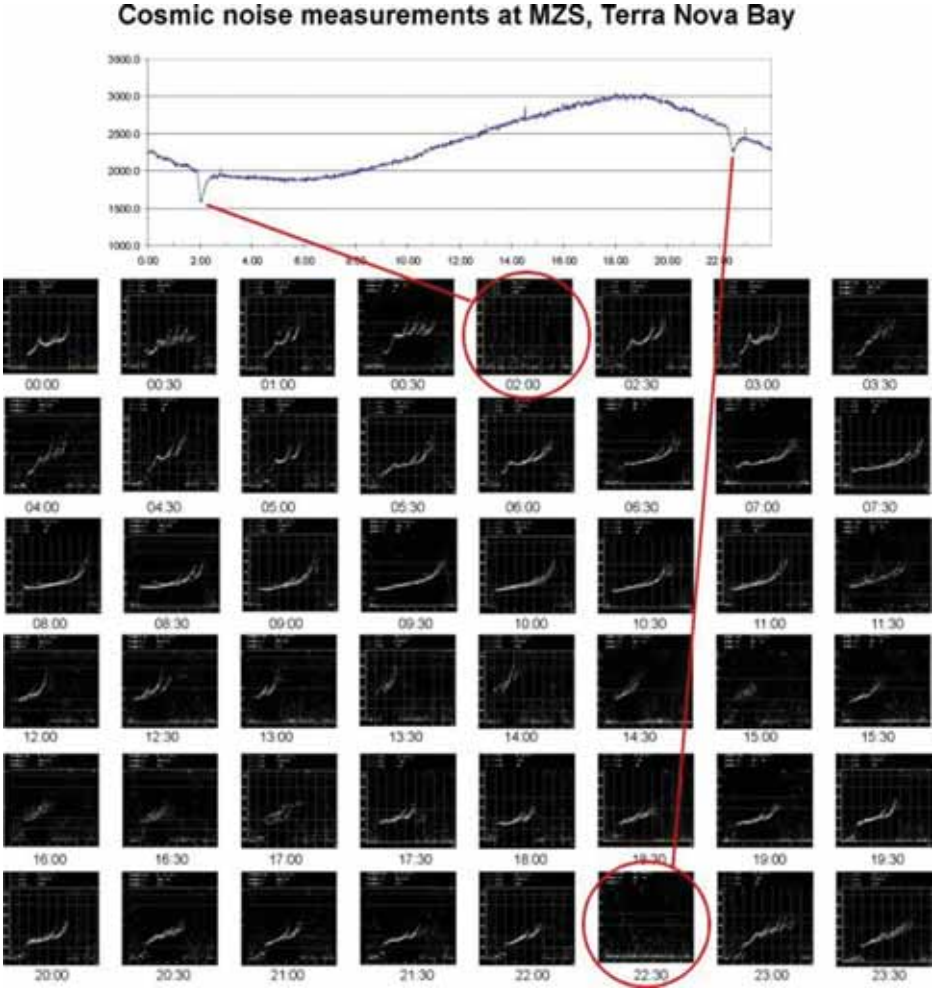

Fig.6. Qualitative comparison between the cosmic noise curve and ionograms recorded respectively by a 30 MHz riometer and by AIS-INGV ionosonde on 26th February 2004.

6. Conclusions and future developments

Results obtained during these first months operation demonstrate that a low-power pulse-compressed ionosonde based on modern radar techniques is suitable for polar ionospheric observations.

In fact the large number of ionograms acquired exhibits well-separated traces from which most of conventional ionospheric parameters can be scaled.

Nevertheless several improvements are necessary for a remote, unmanned observatory like MZS.

First of all, future efforts will be devoted to make the system more robust

and reliable. Particularly system redundancy is required as well as automatic recording of system state parameters such as: temperature, main signals amplitude, matching between the transmitting antenna and the power amplifier.

Another important future aim is to increase the contribution to Space Weather by making scaled parameters from ionograms available in real time. The development of an appropriate automatic scaling program for high latitudes, derived from Autoscala software (Scotto and Pezzopane, 2003), is planned for the future.

7. References

Arokiasamy B.J., C. Bianchi, U. Sciacca, G. Tutone, E. Zuccheretti, 2002. The new AIS-INGV digital ionosonde design report. INGV Internal Technical Report No. 12. (sending an e-mail to ionoinfo@ingv.it a copy of this report can be requested)

Bianchi C., U. Sciacca, A. Zirizzotti, E. Zuccheretti, B.J Arokiasamy, 2003. Signal processing for phase-coded HF-VHF radars. Annals of Geophysics, 46, No. 4, 697-705.

Golay M.J.E., 1961. Complementary series. IRE Transaction on Information Theory, IT-7, N.Y. Institute of Radio Engineers, 82-87.

Hunsucker R.D., 1991. Radio technique for probing the terrestrial ionosphere, Springer Verlag N.Y.

Romano V., M. Cerrone, L. Perrone, M. Pietrella, 2002. Magnetic and solar effects on ionospheric absorption at high latitude. Annals of Geophysics, 45, No. 1, 163-168.

Scotto C., M. Pezzopane, 2002. A software for automatic scaling of foF2 and Muf(3000)F2 from ionograms. Proceedings of URSI 2002, Maastricht,17-24 August 2002, paper 1018 of the electronic copy.

Skolnik M.I., 1981: Introduction to radar systems. Mc Graw Hill N.Y.

Skolnik M.I., 1990. Radar handbook. Mc Graw Hill N.Y.

Zuccheretti E., C. Bianchi, U. Sciacca, G. Tutone, B.J. Arokiasamy, 2003. The new AIS-INGV digital ionosonde. Annals of Geophysics, 46, No. 4, 647-659.

FORECASTING GPS TEC USING THE NEURAL NETWORK TECHNIQUE "A Further Demonstration"

E. Tulunay[1,2], Y. Tulunay[3], E.T. Senalp[1], Lj.R. Cander[4]

[1]Middle East Technical University, Department of Electrical and Electronics Engineering, Inonu Bulvari, 06531, Balgat, Ankara, Turkey, e-mail: ersintul@metu.edu.tr, senalp@metu.edu.tr
[2]TUBITAK Marmara Research Center, Information Technologies Institute, Gebze, Kocaeli, Turkey, e-mail: ersin.tulunay@bte.mam.gov.tr
[3]Middle East Technical University, Department of Aerospace Engineering, Inonu Bulvari, 06531, Balgat, Ankara, Turkey, e-mail: ytulunay@metu.edu.tr
[4]Rutherford Appleton Laboratory, Chilton, Didcot, OXON, OX11 0QX, England, e-mail: l.cander@rl.ac.uk

Abstract. The use of the Middle East Technical University Neural Networks (METU-NN) technique to forecast 10 minute values of the total electron content (TEC), one hour ahead, during high solar activity in the current solar cycle has been demonstrated. Being a data based approach, the METU-NN is trained with the total electron content data evaluated from GPS measurements at Chilbolton (51.8º N; 1.26º W) receiving station for January and February 2000 and 2001. An independent validation data set of the GPS-TEC values for Hailsham (50.9º N; 0.3º E) receiving station for the selected months in 2002 is used as an additional validation to forecast the TEC values one hour in advance.

Key words: Total Electron Content, forecast, Neural Networks, near Earth space, disturbed space weather

1. Introduction

Near-Earth space systems including the ionospheric processes are nonlinear and time varying. Previously it has been demonstrated that Neural Network (NN) based systems are promising in modeling the ionospheric processes (Williscroft and Poole, 1996), (Altinay et al., 1997), (Cander et al., 1998), (Wintoft and Cander, 1999), (Wintoft and Cander, 2000), (McKinnell and Poole, 2000), (Francis et al., 2000), (Tulunay Y. et al., 2001), (Tulunay Y. et al., 2004b), (McKinnell and Poole, 2004).

NN models are especially promising in forecasting applications under disturbed conditions (Tulunay E. et al., 2004) (Stamper et al., 2004). The METU-NN Model was operated in the RAL for forecasting the TEC values 1 hour in advance within the short-term scientific mission of the COST271 Action in July 2002 (COST271 WG 4 STM, 2002).

In this work, a further demonstration of the use of the NN technique for

forecasting GPS TEC during high solar activity in the current solar cycle has been made.

METU-NN models are designed and trained with significant inputs (Tulunay Y. et al., 2004a). In this work, the basic inputs for the model are the temporal inputs, the present TEC value, and its past values up to two hours. In addition, the training, test and validation data are selected so that they contain data from years with similar Sunspot Number values. Thus, the model contains intrinsic information about the solar activity. The METU-NN architecture has one input layer, one hidden layer with the neurons and one output layer. Levenberg-Marquardt Backpropagation Algorithm is used in training the METU-NN models. Then this trained NN is used to forecast the TEC values 1 hour in advance.

This paper outlines the forecast of TEC and preparation of data. It explains the artificial neural network models as a data based approach for forecasting ionospheric processes, gives the results with error tables, cross correlation coefficients and scatter diagrams, and discusses the generalized and fast learning and operation of the METU-NN.

2. Preparation of data

TEC data in 10-minute intervals evaluated from GPS measurements at Chilbolton (51.8^o N; 1.26^o W) receiving station are used for the training, test and validation within the development mode of the METU neural network. The data from selected months in the years 2000 and 2001 are used in the development.

In the operational use, another validation has been performed on an independent validation data set so that the forecast of TEC values for Hailsham (50.9^o N; 0.3^o E) GPS receiving station for selected months in 2002 are made.

Table 1 summarizes the selected train, test and validation time intervals

Table 1. Selection of the time periods for the input data

	Year	Month
Train	2000	Jan and Feb
Test and validation in the development procedure	2001	Jan and Feb
Validation in the operational use	2002	Jan and Feb

In this work the chosen years correspond to similar solar activity. High solar activity times period, i.e. years with similar and high sunspot number values, are selected as train, test and validation years.

3. Construction of the Neural Network based model

The development mode of the METU-NN model consists of "training phase" and "test phase" (Tulunay Y. et al., 2004a). Data sets of the same month but for different years are used for the training and validation phases within the development of the model as shown in Table 1.

Training with a significant and large input database is important in forecast operations. To take advantage of the fast training and applicability with large databases, the "Levenberg-Marquardt Backpropagation" algorithm is used within the training and construction of the METU-NN model. While backpropagation is a steepest descent algorithm, the Levenberg-Marquardt algorithm is an approximation to Newton's method (Hagan and Menhaj, 1994). Newton's method is faster in terms of computation time and more accurate near an error minimum. The Newton's method modification to the steepest descent algorithm, and random initialisations of the model parameters provide the model parameters to reach near global optimum values in the training. To avoid memorization, the validation data are used and the model parameters are recorded when the gradient of the error in the validation phase of the development procedure becomes near zero. To avoid getting stuck in local minima, after the model parameters are recorded the training is continued and it is terminated if the error is an increasing sequence. Otherwise the training is not terminated till the gradient of the error becomes near zero again. Thus, the model parameters are optimized and fixed at the end of the construction procedure. Next, in the operation mode, independent validation data are used for the performance analysis. The errors are calculated, point-by-point, to measure the performance of the METU-NN.

The 8 inputs used for the METU neural network are as follows:

1. The present value of the TEC: $f(k)$,
2. First Difference

$$\Delta_1(k) = f(k) - f(k-60) \tag{1}$$

3. Second Difference

$$\Delta_2(k) = 1(k) - 1(k-60) \tag{2}$$

4. Relative Difference

$$R\Delta(k) = \Delta_1(k) / f(k) \tag{3}$$

5. Cosine component of the minute, m, of the day

$$C_m = -\mathrm{Cos}(2.\pi.m / 1440) \tag{4}$$

6. Sine component of the minute of the day

$$S_m = \mathrm{Sin}(2.\pi.m / 1440) \tag{5}$$

7. Cosine component of the day, d, of the year

$$C_d = -\mathrm{Cos}(2.\pi.d / 366) \tag{6}$$

8. Sine component of the day of the year

$$S_d = \mathrm{Sin}(2.\pi.d / 366) \tag{7}$$

where f(k) is the value of the TEC at the time instant *k* in minutes. TEC values in 10-minute intervals are used. The output is the value of the forecast

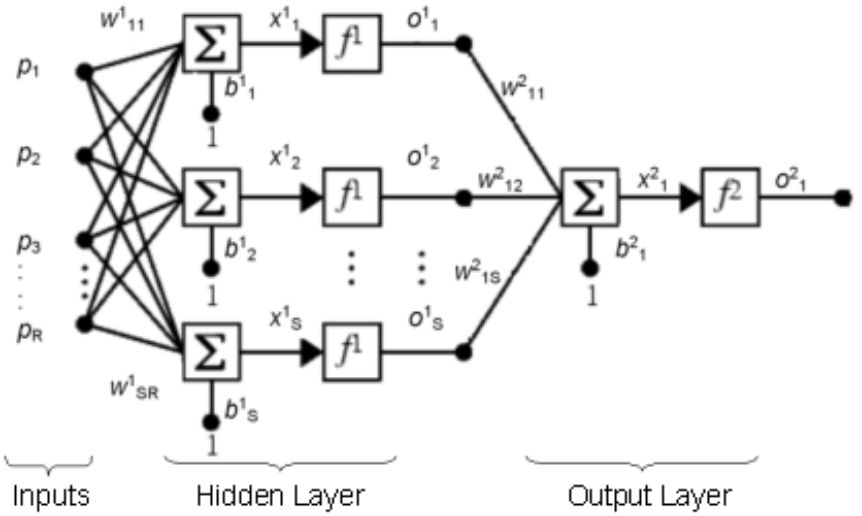

Fig. 1. Architecture of the METU Neural Network model.

TEC to be observed 60 minutes later, i.e. $f(k+60)$. The minus signs in the cosine components have no relevance for the network. They provide graphical and visual insight to the designers and researchers for the temporal inputs.

Among the various NN structures the optimum configuration is found to be the one with 6 hidden neurons in one hidden layer. Consequently, there are 8 inputs, 6 hidden neurons and 1 output in the feed-forward structure. The architecture of the METU-NN model is shown in Figure 1.

The METU-NN indices in Figure 1 are as follows: p_j: j^{th} input to the METU-NN; o^l_i : i^{th} output of the l^{th} layer; b^l_i : i^{th} neuron's bias of the l^{th} layer; w^l_{ij} : weight from neuron j of the l-1^{th} layer to neuron i in the l^{th} layer; f^l : transfer function of the l^{th} layer; x^l_i : sum of the weighted inputs or net output of neuron i of l^{th} layer.

4. Results

In the operation mode, forecast of the TEC values 60 minutes in advance is performed for the validation data set in 10-minute intervals. Then cross correlations of observed and forecast TEC values are calculated. Also the root mean square, normalized and absolute error values are calculated. The analysis and results of the TEC forecast, which are shown in Table 2, cover the time interval between January and February 2002 for the Hailsham receiving station.

Figure 2 shows the TEC values versus the order of data points in January and February 2002. The 1-hour advance forecast values of the TEC in a solid line are superimposed on the observed GPS-TEC values (dashed line).

Table 2. Error Table

Root Mean Square Error (TECU)	2.6122
Normalized Error	0.0789
Absolute Error (TECU)	1.7810
Cross Correlation Coefficient	0.9943

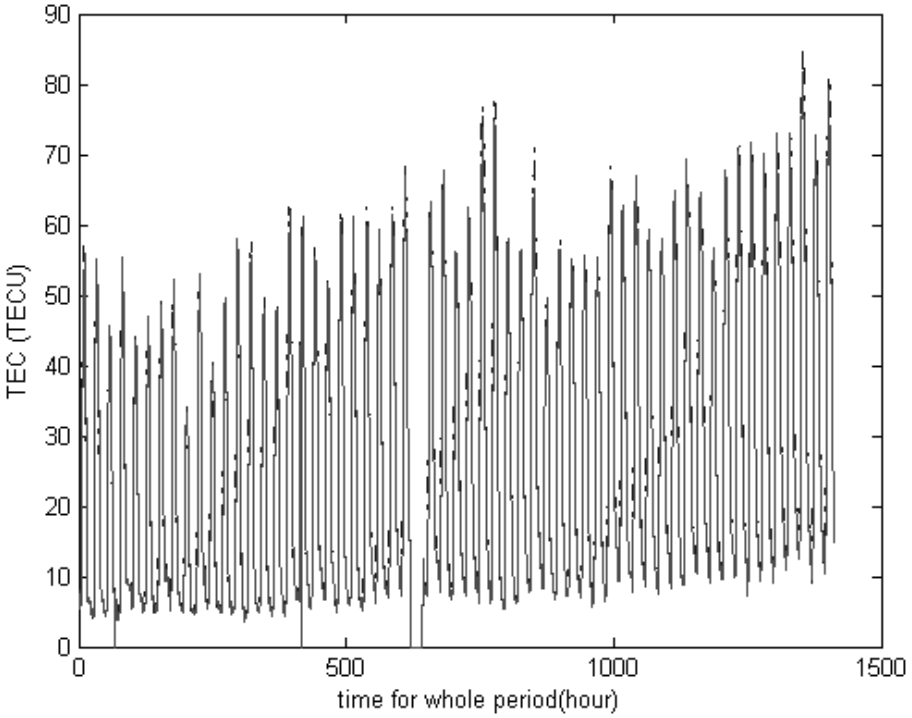

Fig. 2. Observed GPS TEC results (dotted), 1 hour ahead Forecast (solid) TEC values for the whole time of validation period: January-February 2002 for Hailsham.

Figure 3 is the scatter diagram of the forecast and observed TEC values for January and February 2002.

The cross correlation coefficient between the observed and forecast TEC values is 0.9943 and the deviations from the best-fit line in the scatter diagram are small. The lower bound 0.9941, and the upper bound 0.9946 are the 95% confidence limits, i.e. the level of significance is $\alpha=0.05$ (Spiegel et al., 2000). Consequently, the METU-NN model learned the shape of the inherent non-linearities. Also the fitted line has a slope close to 45 and it passes through the origin. As a result the forecasting errors are small and the neural network system reached the correct operating point.

To illustrate how the model can perform two solar events, which took place outside of the training period, were considered. That is, the Coronal Mass Ejection (CME) events of January the 4th and February the 12th of

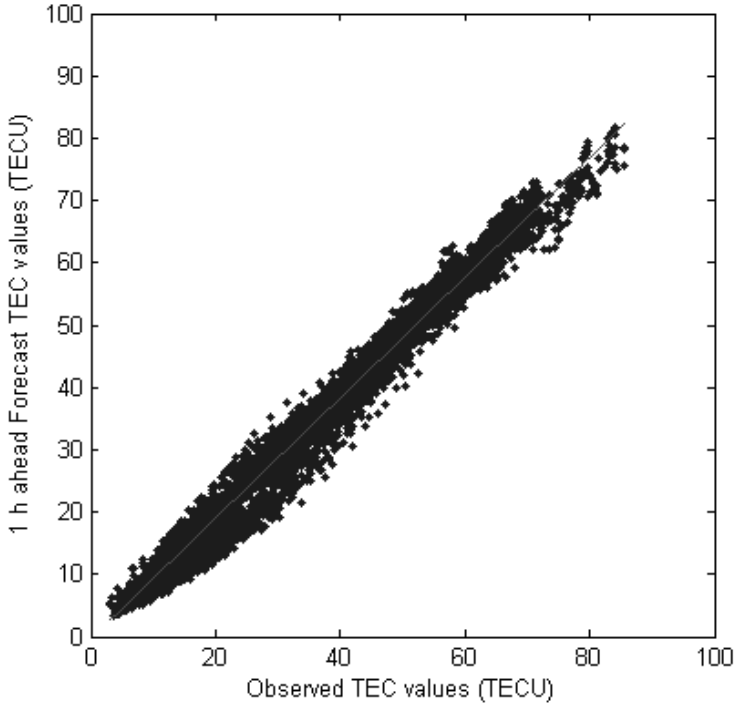

Fig. 3. 1 hour ahead Forecast TEC values versus Observed GPS TEC results (dots) with the linear fit line for the whole time of validation period: January-February 2002 for Hailsham.

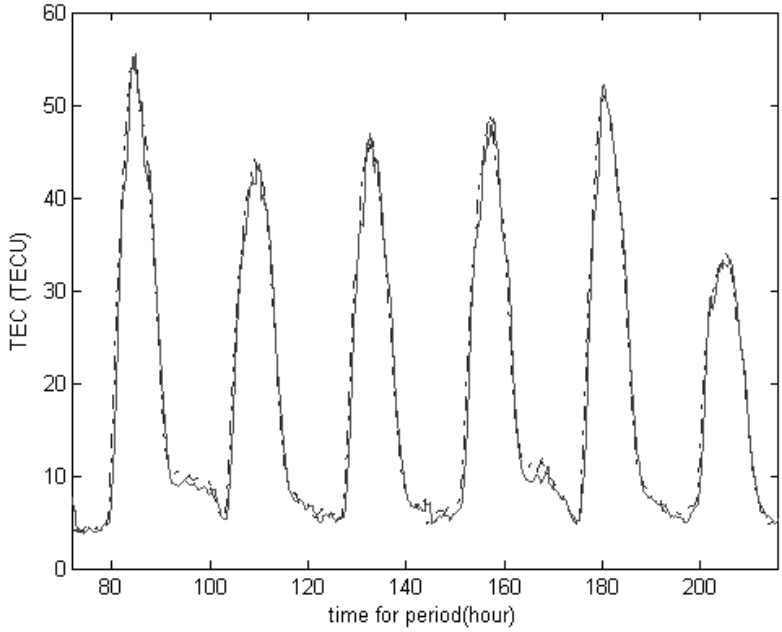

Fig. 4. Observed GPS TEC results for disturbed solar-terrestrial conditions (dotted), and 1 hour ahead Forecast (solid) TEC values for the enlarged section of the time of validation period: 4-9 January 2002.

2002 are two major solar events that occurred within the time interval of the validation data. Large Angle and Spectrometric Coronagraph Experiment (LASCO) and the Solar and Heliospheric Observatory (SOHO) Extreme ultraviolet Imaging Telescope (EIT) observed a full halo CME on 4 January 2002 (LASCO, 2002). It had an earthward component so that it looks roughly like a halo or ring around the Sun. Also EIT and LASCO observed another CME on 12 February 2002 (LASCO, 2002).

Figures 4 and 5 are enlarged sections of the data points shown in Figure 2, i.e. the diurnal variations of the observed, and forecast TEC values during 4-9 January 2002 and 12-15 February 2002 respectively.

In Figures 2, 3, and in the enlarged sections of Figure 2, i.e. Figures 4 and 5, it can be observed that the performance of forecasting the GPS-TEC values by using the METU-NN model is high.

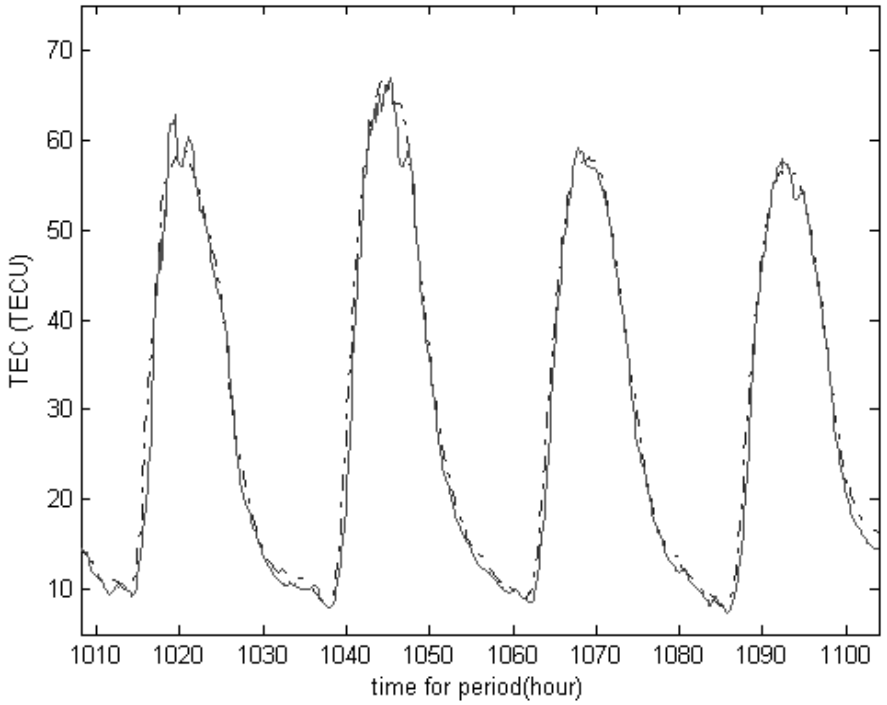

Fig. 5. Observed GPS TEC results for quiet solar-terrestrial conditions (dotted), and 1 hour ahead Forecast (solid) TEC values for the enlarged section of the time of validation period: 12-15 February 2002.

5. Conclusions

Forecasting of the TEC values, especially in disturbed space weather conditions, is crucial for communication, radar and navigation systems employing HF radio waves to cope with the effects of the unpredictable variability of ionospheric parameters.

In this work forecasting of an ionospheric-plasmaspheric process, the TEC variation, was made 1 hour in advance by using neural network based

METU-NN model. In the training phase, the model learned the shape of the complex nonlinearities in the process and the METU-NN parameters reached the values for the correct operating point of the system.

As a general conclusion, it is shown that properly constructed neural network based systems, trained and tested with properly organized data, are promising in modeling the complex nonlinear processes, such as the TEC variation.

Summarizing, the main contributions of this work are as follows:

1) Organization of representable data for teaching complex processes,

2) Neural network based identification of a highly complex nonlinear process such as the TEC variation, and

3) General demonstration of the learning capability by calculating cross correlations and reaching a proper operating point by calculating errors.

6. References

Altinay O., E.Tulunay, Y. Tulunay, 1997. Forecasting of ionospheric critical frequency using neural networks, Geophysical Research Letter, 24, No. 12, 1467-1470, and COST251 TD(96)016.

Cander Lj.R., M.M. Milosavlijevic, S.S. Stankovic, S. Tomasevic, 1998. Ionospheric Forecasting Technique by Artificial Neural Network, Electronics Letters, 34, No. 16, Online No: 19981113, 1573-1574.

COST271 WG 4 STM, 2002. Effects of the Upper Atmosphere on Terrestrial and Earth-Space Communications, Short term scientific mission work on the TEC data available at RAL to organize the input data for the METU NN model by E.T. Senalp under the supervision of Dr. Lj. Cander, Terms of Reference, COST 271 Action, WG 4, 30 June 2002 - 7 July 2002, RAL, Chilton, Didcot, U.K.

Francis, N.M., P.S. Cannon, A G Brown, D S Broomhead, 2000. Nonlinear prediction of the ionospheric parameter foF2 on hourly, daily, and monthly timescales., J. Geophys. Res., 105, No. A6, 12839-12849.

Hagan M.T., M.B. Menhaj, 1994. Training Feedforward Networks with the Marquard Algorithm, IEEE Transactions on Neural Networks, 5, No. 6, 989-993.

LASCO web site, 2002. Large Angle and Spectrometric Coronagraph Experiment (LASCO) and Solar and Heliospheric Observatory (SOHO (ESA & NASA)) Extreme ultraviolet Imaging Telescope (EIT) instruments, Coronal Mass Ejections, the SOHO/LASCO data produced by a consortium of the Naval Research Laboratory (USA), Max-Planck-Institut fuer Aeronomie (Germany), Laboratoire d'Astronomie (France), and the University of Birmingham (UK)., http://lasco-www.nrl.navy.mil/.

McKinnell L.A., A.W.V. Poole, 2000. The development of a Neural Network based short term foF2 forecast program, Phys. Chem. Earth, Part C, 25, No. 4, 287-290.

McKinnell L.A., A.W.V. Poole, 2004. Predicting the ionospheric F layer using neural networks, J. Geophys. Res., 109, No. A8, A08308, doi:10.1029/2004JA010445.

Spiegel M.R., J. Schiller, R.A. Srinivasan, 2000. Schaum's Outline of Theory and Problems of Probability and Statistics, 2nd ed., 206-209, 287-288, 313-314, McGraw-Hill, New York, USA.

Stamper R., A. Belehaki, D. Buresova, Lj.R. Cander, I. Kutiev, M. Pietrella, I. Stanislawska, S. Stankov, I. Tsagouri, Y.K. Tulunay, B. Zolesi, 2004. Nowcasting, forecasting and warning for ionospheric propagation: tools and methods, Annals of Geophysics, 47, No. 2/3, 957-983.

Tulunay E., E.T. Senalp, Lj.R. Cander, Y.K. Tulunay, A.H. Bilge, E. Mizrahi, S.S. Kouris, N. Jakowski, 2004. Development of algorithms and software for forecasting, nowcasting and variability of TEC, Annals of Geophysics, 47, No. 2/3, 1201-1214.

Tulunay Y., E. Tulunay, E.T. Senalp, 2001. An Attempt to Model the Influence of the Trough on HF Communication by Using Neural Network, Radio Science, 36, No. 5, 1027-1041.

Tulunay Y., E. Tulunay, E.T. Senalp, 2004a. The Neural Network Technique-1: A General Exposition, Adv. Space Res., 33, No. 6, 983-987.

Tulunay Y., E. Tulunay, E.T. Senalp, 2004b. The Neural Network Technique-2: An Ionospheric Example Illustrating its Application, Adv. Space Res., 33, No. 6, 988-992.

Williscroft L.A., A.W.V. Poole, 1996. Neural Networks, foF2, sunspot number and magnetic activity, Geophys. Res. Lett., 23, No. 24, 3659-3662.

Wintoft P, Lj.R. Cander, 1999. Short term prediction of foF2 using timedelay neural networks, Phys. Chem. Earth, Pt C, 24, No. 4, 343-347.

Wintoft P, Lj.R. Cander, 2000. Ionospheric foF2 storm forecasting using neural networks, Phys. Chem. Earth, Pt C, 25, No. 4, 267-273.

In Memoriam

SOPHIA KONYAROVA - KLEVTSOVA
1942 - 2004

Almost an year has passed since the decease of our Editorial Secretary (ES) Sophia Konyarova Klevtsova, whom everybody knew and called just Sonia. She was a devoted and loved colleague, working at the Geophysical Institute since 1968, after graduating the Sofia University. When English language was not that popular in Bulgaria, Sonia started teaching specialized English classes for many our scientist. She also cooperated for the establishment of valuable contacts between Bulgarian scientists and their colleagues from abroad.
During all these years she was recognized as a popular interpreter, translator and editor of scientific publications. Her colleagues and friends at the Geophysical institute will always remember her with love. She was always cheerful, warm-hearted and helped us a lot in our work. She translated, edited and prepared all articles that had to be published in English with utmost care to the smallest detail.
As a very sociable person, she was also a wanted organizer of scientific forums in Earth Science. As an ES, her efforts were recognized in the preparation of the Bulgarian Geophysical Journal, which added to the popularization of the Bulgarian Geophysical science.
She never forgot her colleagues and friends from near and distant countries, with whom she kept good correspondence and contacts.
Let us remember Sonia with love!

From her colleagues

Supplement

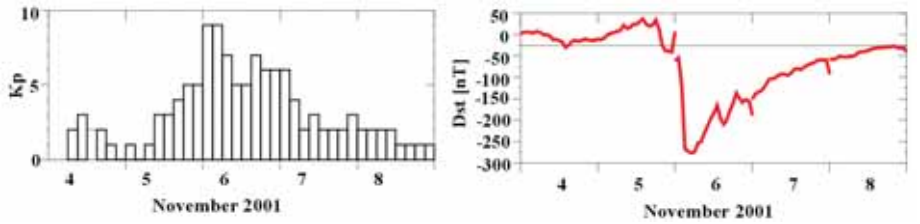

Fig.1. Variations of Kp and Dst index during 4 - 8 November 2001.

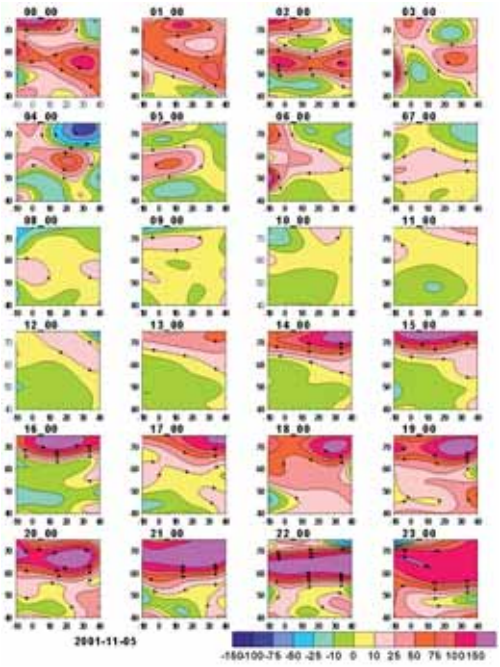

Fig.3a. The differential TEC maps over Europe for 5 November 2001

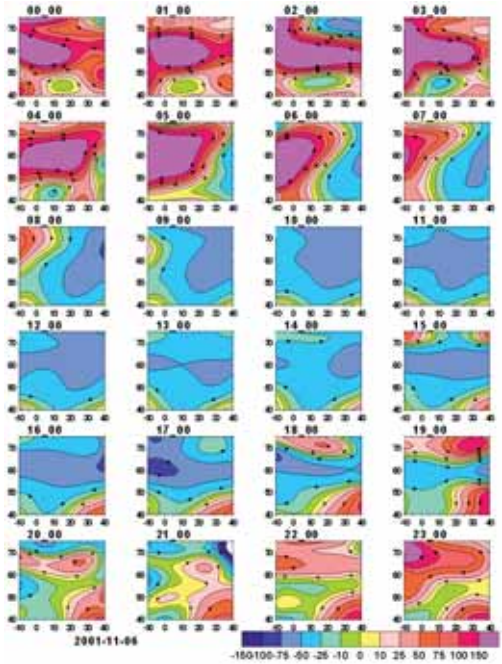

Fig.3b. The differential TEC maps over Europe for 6 November 2001.

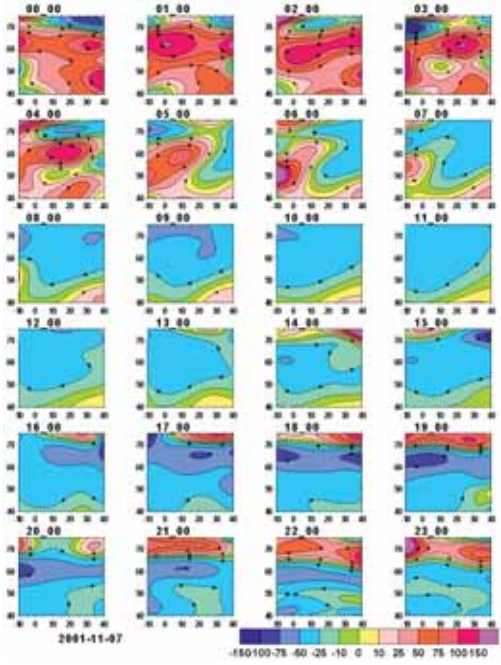

Fig.3c. The differential TEC maps over Europe for 7 November 2001.

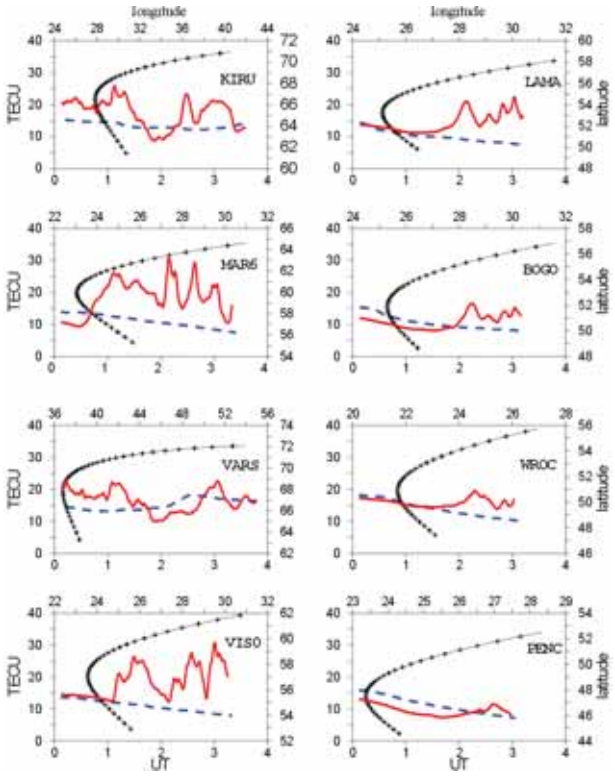

Fig 4. Temporal TEC variations along individual satellite passes for PRN 14 observed at different stations on quiet (blue) and disturbed (red) day.

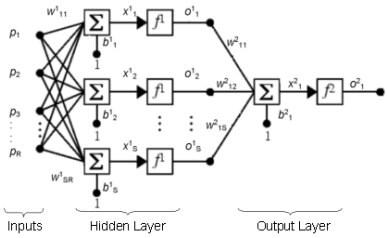

Fig. 1. Scenario of GPS navigation measurements onboard CHAMP and SAC-C.

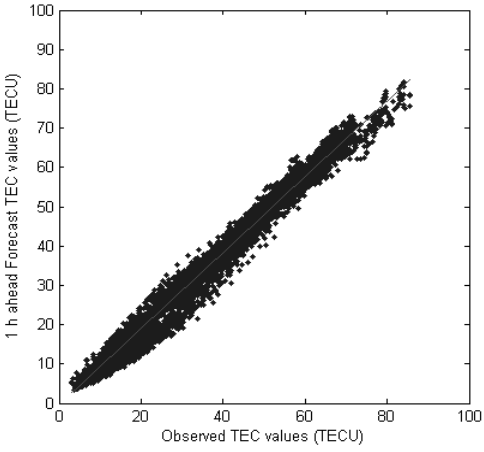

Fig. 3. Scheme of data flow and processing for reconstruction of electron density distributions from CHAMP and SAC-C GPS navigation measurements

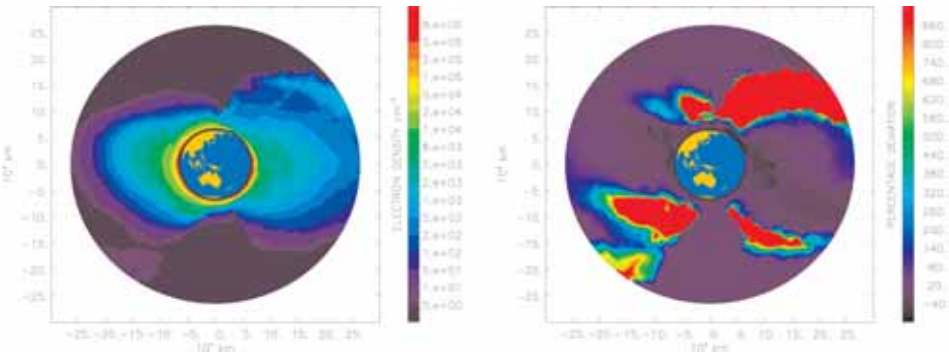

Fig. 6. Meridional slices in the CHAMP orbit plane (along 233° E, local time 22:30), assimilation example for October 27, 2002, Begin of assimilation: 06:13 UT, duration: 93 minutes. Left panel: Reconstruction of the ionospheric/plasmaspheric electron density distribution after the assimilation of TEC data from CHAMP and SAC-C (full CHAMP revolution). Right panel: Percentage deviation of the assimilation result from the initial model (PIM).

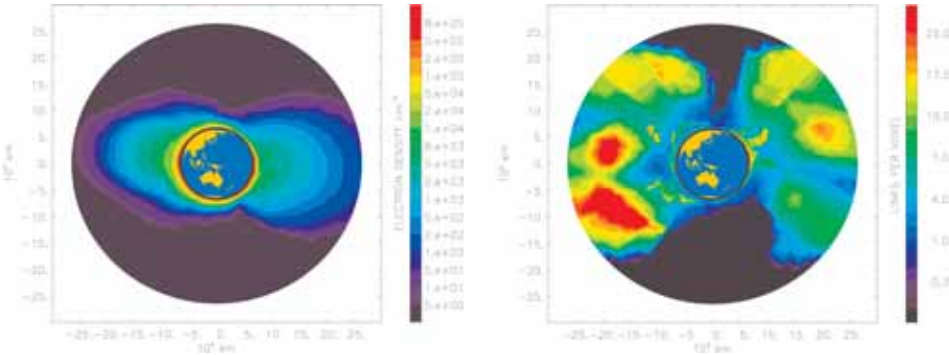

Fig. 7. Meridional slices in the CHAMP orbit plane, same assimilation example as shown in Fig. 6 but using only CHAMP TEC data. Left panel: Reconstruction of the ionospheric/plasmaspheric electron density distribution. Right panel: Corresponding data coverage

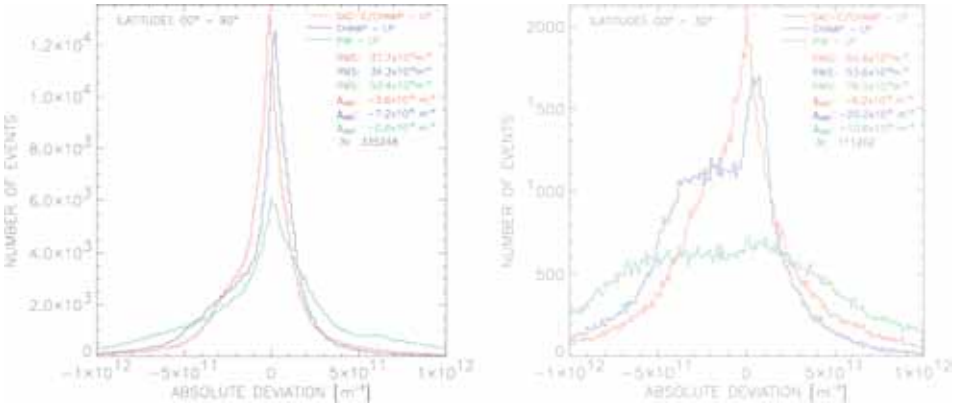

Fig. 8. Electron density comparisons for 2002, days of the year 36-47, 166-176, 293-309. Absolute deviations between CHAMP Langmuir Probe (LP) and: CHAMP/SAC-C assimilation, pure CHAMP assimilation and PIM. Left panel: global comparison. Right panel: low latitudes only (0° till 30° latitude, both hemispheres).

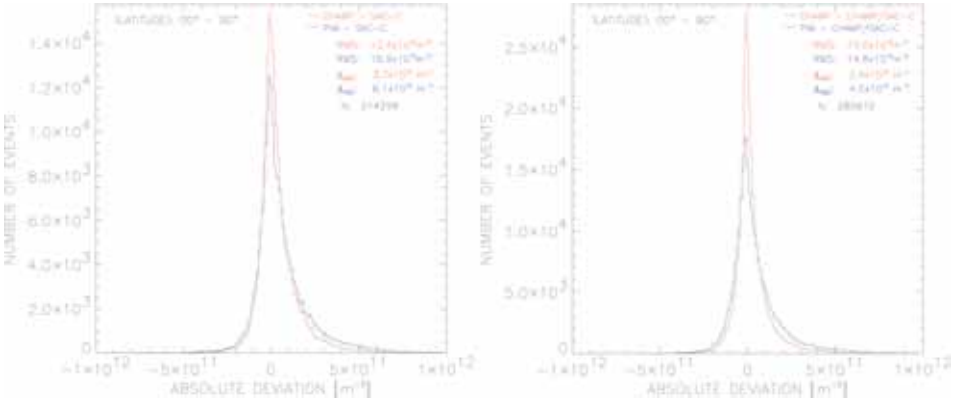

Fig. 9. Electron density comparisons along SAC-C path for 2002, days of the year 36-47, 166-176, 293-309. Left panel: Absolute deviation between pure CHAMP and SAC-C assimilation and between PIM and SAC-C assimilation. Right panel: Same as left panel but CHAMP/SAC-C in place of pure SAC-C assimilation.

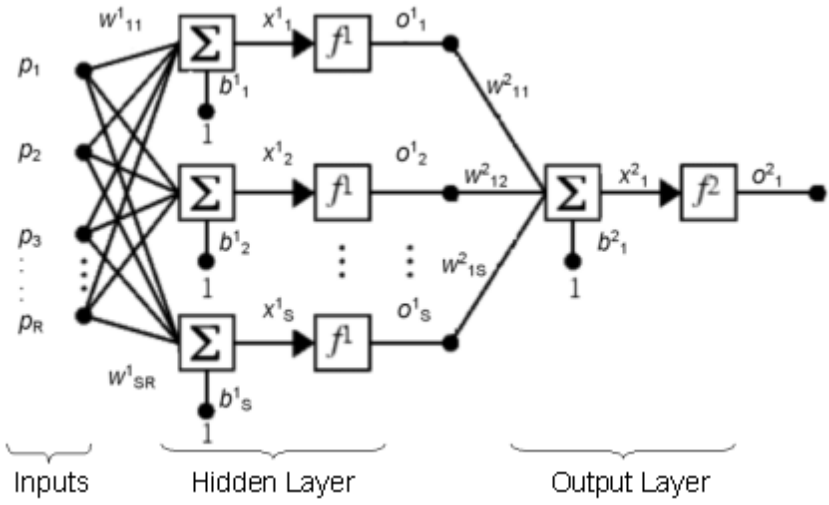

Fig. 1. Deciles of variability in foF2 (Rome) from hourly daily measurements (black) and from measurements every 10-minutes (red).

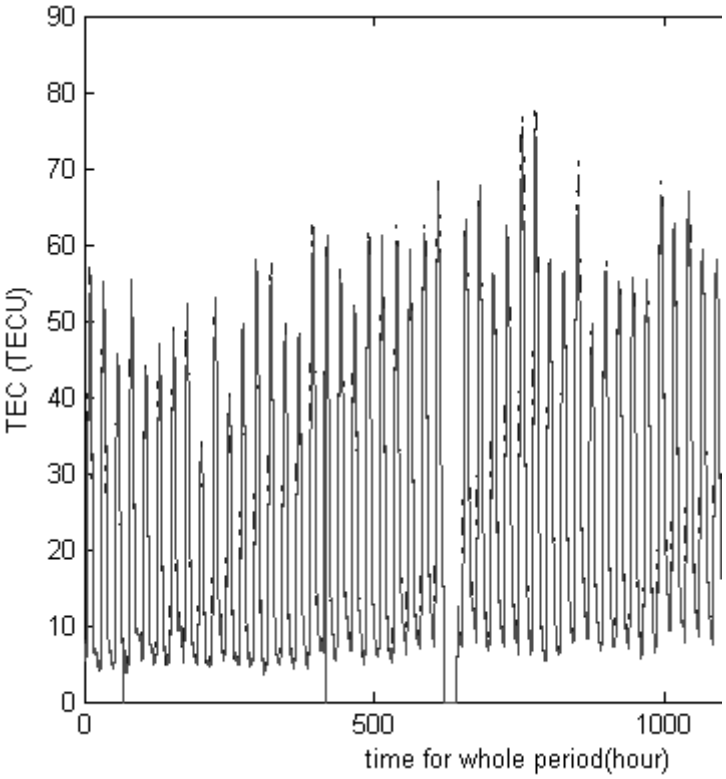

Fig. 2. Deciles of variability in TEC (Matera) from hourly daily data (black) and TEC-data measured every 10-minutes (red).

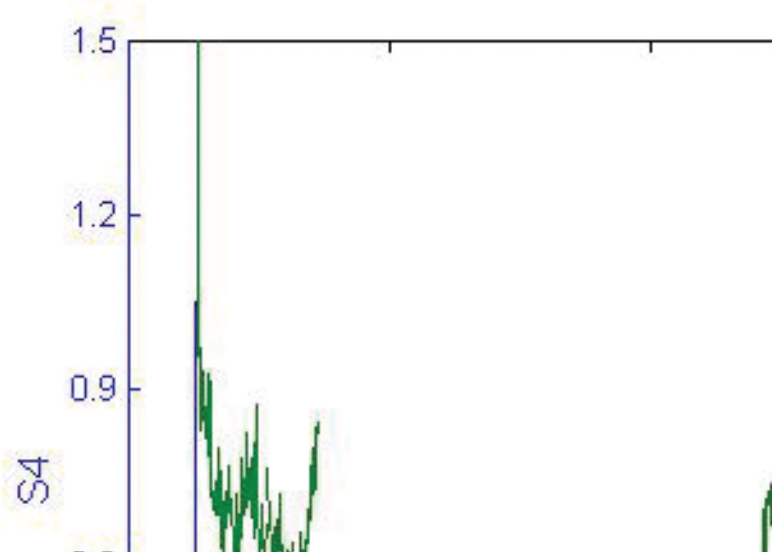

Fig. 3a. Variability within-the-hour of TEC from 10-min. measurements using eq. (1).

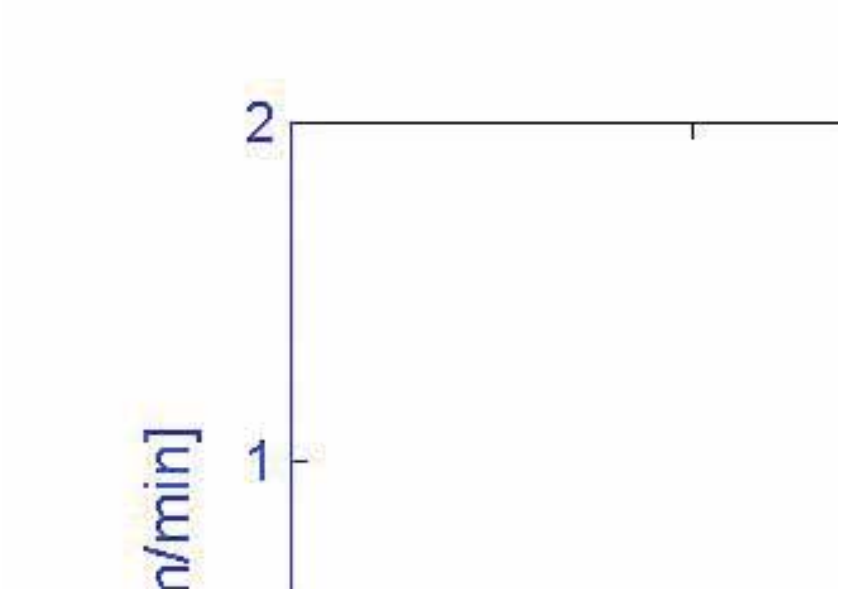

Fig. 3b. Variability within-the-hour of foF2 from 10-min. measurements.

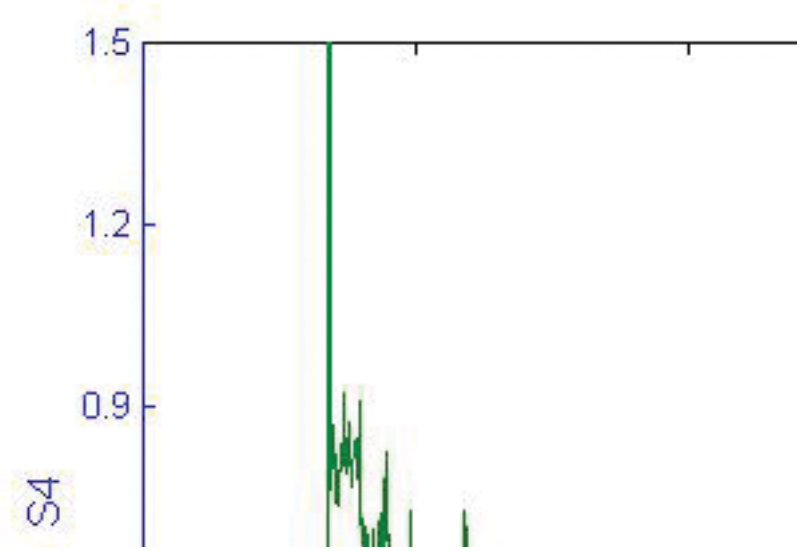

Fig.4a. Variability within-the-hour of TEC from 10-min. measurements using eq. (1).

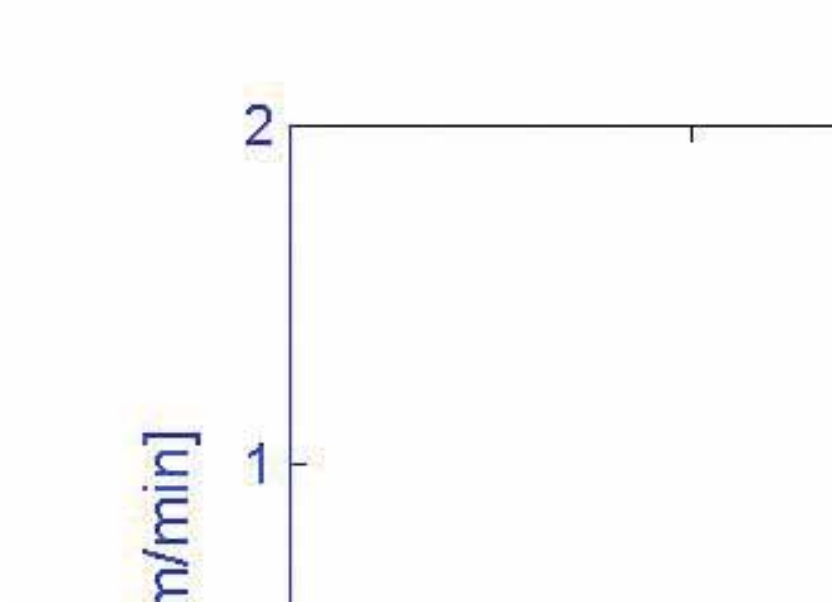

Fig. 4b. Variability within-the-hour of foF2 from 10-min. measurements.

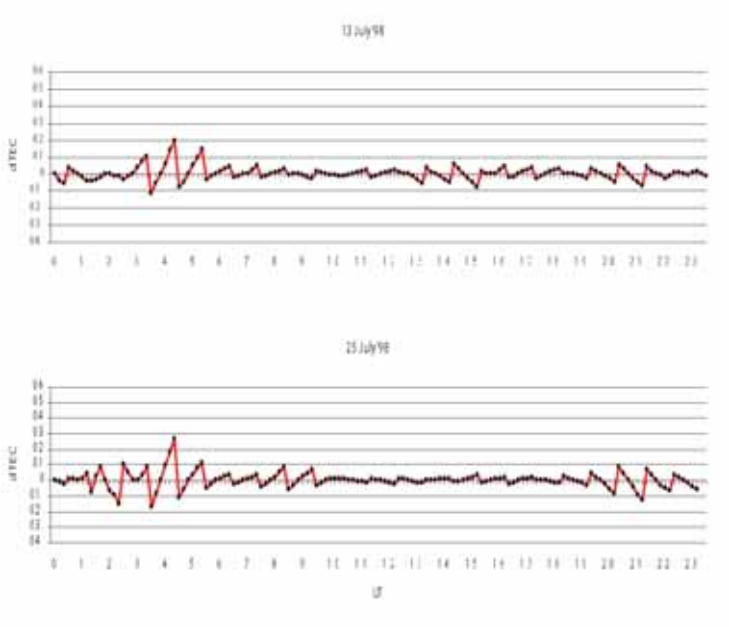

Fig.5a. Variability within-the-hour of TEC from 10-min. measurements using eq. (1).

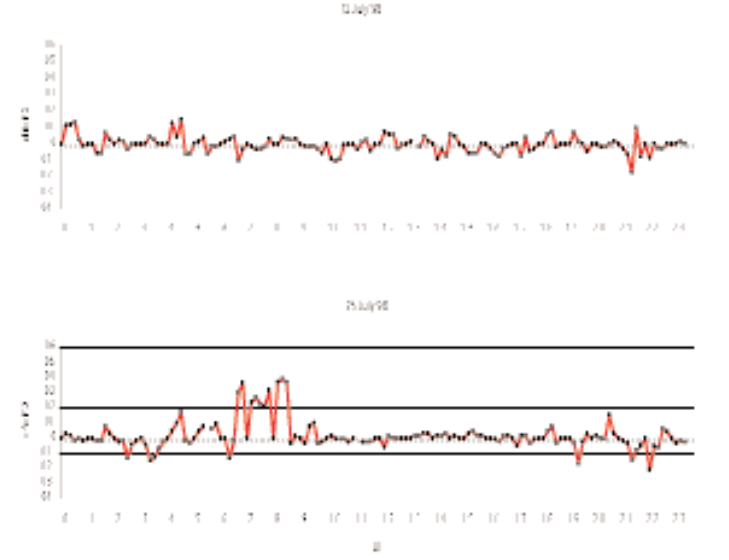

Fig.5b. Variability within-the-hour of foF2 from 10-min. measurements

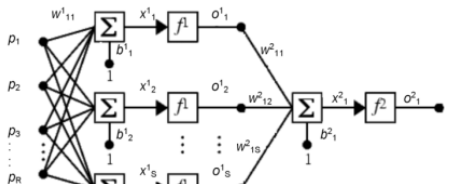

Fig. 1. Dst index during October 2003, as released by Kyoto University

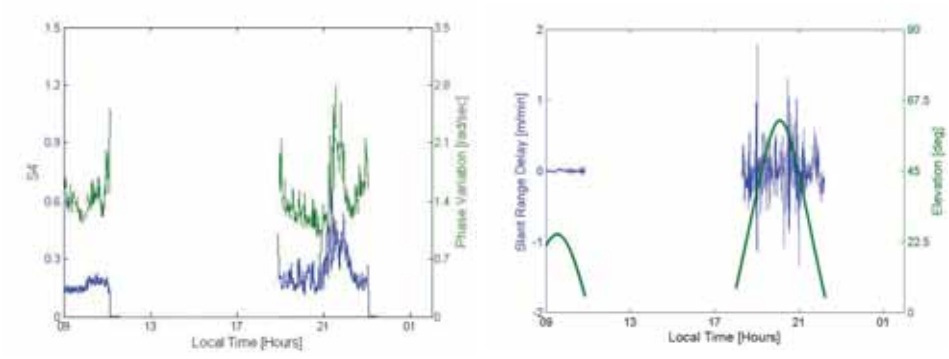

Fig. 2. (a) S_4 scintillation index (blue curve) and S_ϕ phase scintillation index (i.e., phase variation) in rad/sec (green curve) for PRN03, during 30-Oct.-2003; (b) TEC f;luctuations in L1 range equivalent (blue curve) in m/min and elevation angle (green dots) for PRN03, during 30-Oct.-2003.

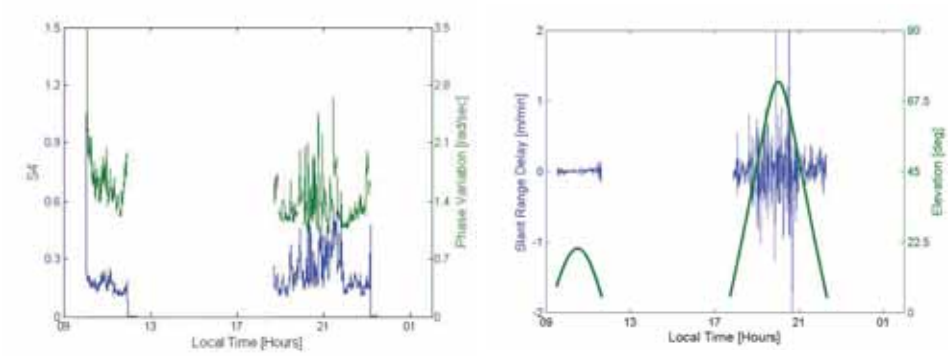

Fig. 3. (a) S_4 scintillation index (blue curve) and S_ϕ phase scintillation index (i.e., phase variation) in rad/sec (green curve) for PRN15, during 30-Oct.-2003; (b) TEC f;luctuations in L1 range equivalent (blue curve) in m/min and elevation angle (green dots) for PRN03, during 30-Oct.-2003.

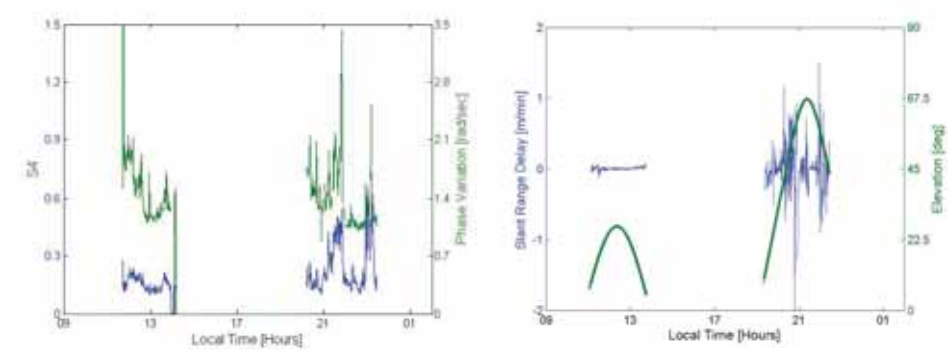

Fig. 4. (a) S_4 scintillation index (blue curve) and S_ϕ phase scintillation index (i.e., phase variation) in rad/sec (green curve) for PRN23, during 30-Oct.-2003; (b) TEC f;luctuations in L1 range equivalent (blue curve) in m/min and elevation angle (green dots) for PRN03, during 30-Oct.-2003.

Fig.1. Geographical location of the Italian Antarctic Base

Fig.3. The Italian Antarctic ionospheric observatory.

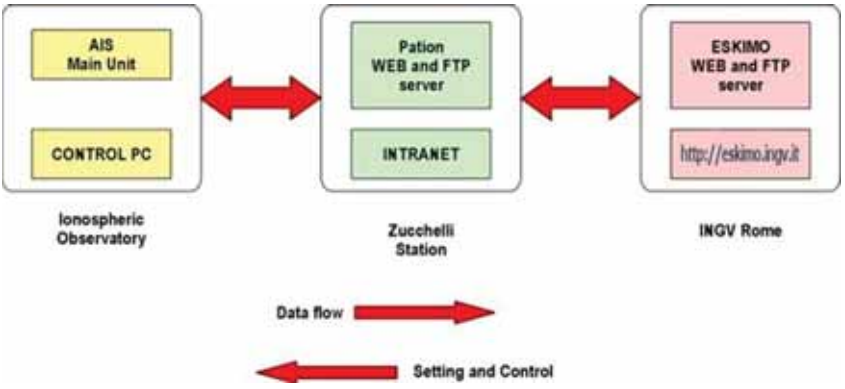

Fig.4. Diagram showing the AIS-INGV ionosonde data flow.

Bulgarian Geophysical Journal (BGJ) is an interdisciplinary journal containing original contributions on the atmosphere and space physics, geomagnetism and gravimetry, seismology and physics of the Earth's interior, as well as those dealing with applied geophysics, instrumentation and observations in these scientific fields. BGJ publishes research papers, brief reports and comments on current research and is organized along the four disciplinary lines. BGJ is published in 4 issues per year.

Address of the Editorial Board:
Bulgarian Geophysical Journal, Geophysical Institute, Acad.G.Bonchev Street, bl.3, Sofia1113, Bulgaria,
e-mail: bgj@geophys.bas.bg
Editorial Secretary: S.Koniarova-Klevtzova
Technical Editor: N. Ninova, tel. 979 3946

2002
55 (05)
Bulgarian Academy of Sciences
Printed in: "xxxxx", Sofia, Bulgaria

Information for Contributors

Submission of a paper implies that it has not been published previously and is not under consideration for publication elsewhere.

Typescript. All parts of the paper must be typed double-spaced on good quality white paper A4 (210 x 297mm) with at least 2.5 cm margins at top, bottom, and sides. Each page of the typescript should be numbered in the top right hand corner.

Authors are expected to supply 2 clean copies in English and when possible one in Bulgarian. Please use correct English spelling, punctuation, grammar, and syntax. The metric system must be used throughout; use of appropriate SI units is encouraged.

Paper length. Paper should be written in the most concise form. Occasionally long papers (over 15p.) are accepted, particularly those of a review nature.

The typescript should be arranged as follows:

1. Title page including authors' names and affiliations
2. Abstract and key words
3. Text (including tables and figures)
4. Reference list

Abstract. The abstract should be in a single paragraph (250 words or fewer). State the nature of the investigation and summarize its important conclusions. References must not be cited in the abstract. The abstract should be suitable for separate publication in a Web site.

Mathematics. All characters available on a standard typewriter must be typewritten in the equations as well as in text. Special attention should be paid to single couples of the kind: vv, pp, mμ, nη. Distinction should be made between the letter O and the numeral 0; between the letter l and the numeral 1; between k and kappa.

Alignment of symbols must be unambiguous. Superscripts and subscripts should clearly be in superior or inferior position. Fraction bars should extend under the entire numerator. Displayed equations should be numbered consecutively throughout the paper; the number (in parentheses) should be to the right of the equation.

References. A complete and accurate reference list is of major importance. Only works cited in the text should be included in the reference list. References are cited in the text by the last name of the author and the year: (Jones, 1990). If the author's name is part of the sentence, only the year is bracketed. References are arranged alphabetically by the last names of authors. Multiple entries for a single author are arranged chronologically. Two or more publications by the same author in the same year are distinguished by a, b, c after the year.

Tables. Tables should be typed as authors expect them to look in print. Every table must have a title. Column headings must be arranged so that their relation to the data is clear. Each table must be cited in the text.

Illustrations. All illustrations should be inserted in the text, suitable for the camera-ready reproduction (which may include reduction). Each figure must be cited in numerical order in text and must have figure legend. Please do not draw with hairlines. The minimum line width is 0.2 mm (i.e. 0.567pt).

Electronic submission. Authors must submit an electronic copy of their paper with the final version of the manuscript. The electronic copy should match the hardcopy exactly.

Authors will receive more detailed information when the article is accepted for publication so that requirements for the camera-ready presentation are fulfilled.